bioRxiv preprint doi: https://doi.org/10.1101/2021.06.09.447757; this version posted June 9, 2021. The copyright holder for this preprint (which was not certified by peer review) is the author/funder. All rights reserved. No reuse allowed without permission.

Nanoparticle-delivered palbociclib enable CDK4/6 inhibitor therapy while combination with mTORC1 inhibitor sapanisertib induces long term benefits in SHH medulloblastoma.

Authors: Chaemin Lim[1]†, Taylor Dismuke[2]†, Daniel Malawsky[3,4], Jacob D. Ramsey[1], Duhyeong Hwang[1], Virginia L. Godfrey[4], Alexander V. Kabanov[1,5], Timothy R. Gershon [3,6,7]* and Marina Sokolsky-Papkov[1]*

Affiliations:
[1] Center for Nanotechnology in Drug Delivery and Division of Pharmacoengineering and Molecular Pharmaceutics, Eshelman School of Pharmacy, University of North Carolina at Chapel Hill, NC 27599, U.S.A.

[2]Department of Pathology, UNC School of Medicine, University of North Carolina at Chapel Hill, NC 27599, USA
[3] Department of Neurology, UNC School of Medicine, University of North Carolina, Chapel Hill, NC 27599, USA.
[3] Wellcome Sanger Institute, Hinxton, Cambridgeshire, UK
[4] Department of Pathology and Laboratory Medicine, University of North Carolina, Chapel Hill, NC 27599, USA.
[5] Laboratory of Chemical Design of Bionanomaterials, Faculty of Chemistry, M.V. Lomonosov Moscow State University, Moscow, 119992, Russia.
[6] Lineberger Comprehensive Cancer Center, University of North Carolina, Chapel Hill, NC 27599, USA.
[7] Neuroscience Center, University of North Carolina, Chapel Hill, NC 27599, USA.

*Corresponding author. Email: gershont@neurology.unc.edu (T.R.G.); msokolsk@email.unc.edu (M.SP)

† These authors contributed equally to this work

One Sentence Summary: Nanoparticle-delivered palbociclib enable CDK4/6 inhibitor therapy while combination with mTORC1 inhibitor sapanisertib induces long term benefits in SHH medulloblastoma.

bioRxiv preprint doi: https://doi.org/10.1101/2021.06.09.447757; this version posted June 9, 2021. The copyright holder for this preprint (which was not certified by peer review) is the author/funder. All rights reserved. No reuse allowed without permission.

Abstract

While targeting CDK4/6 is highly effective in breast cancer and is a promising approach for brain tumor treatment, palbociclib, FDA-approved CDK4/6 inhibitor, failed to induce durable benefits in preclinical models of brain cancers (intrinsic pontine glioma and medulloblastoma) and in clinical trial against glioblastoma. In our study in transgenic, medulloblastoma-prone mice, orally dosed palbociclib induces no benefits. However, nanoparticle formulation of palbociclib, POx-Palbo enables systemic administration of the drug, improves CNS pharmacokinetics and induces survival benefit. In addition, we analyzed the response to the POx-Palbo treatment using scRNA-seq to identify treatment targets in palbociclib resistant cells. In parallel, we tested the potential of agents targeting SHH signaling or DNA replication to limit resistance, identifying combination regiment of palbociclib and etoposide which slightly improved efficacy. The brains of mice repeatedly treated with POx-Palbo showed a distinct population of proliferating cells cluster with a transcriptomic profile that was different from proliferating cells in control tumors. With Gene Ontology (GO) enrichment analysis of the genes in each cluster, we found that POx-Palbo treatment increased the expression of the glutamate transporter Slc1a2 and decreased diverse ribosomal genes, which both are indicating the inhibition of mTORC1 signaling pathway. Treatment with small molecule mTORC1 inhibitor, sapanisertib, induced survival benefits and the combination of palbociclib and sapanisertib markedly increased anti-tumor efficacy and survival with dramatic suppression of phosphorylation in RB and 4EBP1, indicating a potentially effective new therapy for pediatric medulloblastoma.

bioRxiv preprint doi: https://doi.org/10.1101/2021.06.09.447757; this version posted June 9, 2021. The copyright holder for this preprint (which was not certified by peer review) is the author/funder. All rights reserved. No reuse allowed without permission.

INTRODUCTION

Patients with medulloblastoma, the most common malignant brain tumor in children, need new therapies. The current standard treatment for medulloblastoma with surgery, craniospinal radiation (xRT) and chemotherapy cures ~80% of patients, but causes disabling untoward effects, including neurocognitive impairment, hearing loss, endocrine dysfunction and secondary malignancies. Survivors remain at risk of recurrence after treatment, and recurrent medulloblastoma is presently incurable. Therapies that specifically target the biology of the tumor and spare normal tissues may improve the efficacy of medulloblastoma therapy and decrease long-term toxicities.

CDK4/6 inhibitors may be ideal targeted agents for medulloblastoma (*1*, *2*). While medulloblastomas are a heterogeneous group of tumors with 4 subgroups, all 4 groups of medulloblastomas typically disable the RB tumor suppressor through CDK4/6-mediated RB phosphorylation (pRB) and *RB* mutations are rare in every subgroup (*3*-*5*). The CDK4/6 inhibitor palbociclib (Ibrance, Pfizer, Inc.) effectively blocks RB phosphorylation and arrests cells with intact RB in the G_1 phase of the cell cycle (*6*) and is FDA-approved for specific breast cancers, in combination with hormonal therapy (*7*, *8*).

Optimizing palbociclib for medulloblastoma therapy may require both improved CNS pharmacokinetics (PK) and identifying mutually enhancing drug combinations. The brain penetration of palbociclib is limited (*9*), and dose-limiting toxicities restrict the potential for increasing systemic doses to improve drug delivery to the CNS. Moreover, genetic deletion studies show that cells in *Cdk4/6*-deleted mice are able to progress through the cell cycle both *in vivo* and *in vitro*, indicating that alternative mechanisms can substitute for CDK4/6 activity (*10*). These mechanisms may support palbociclib resistance, and combinations of drugs are needed to

bioRxiv preprint doi: https://doi.org/10.1101/2021.06.09.447757; this version posted June 9, 2021. The copyright holder for this preprint (which was not certified by peer review) is the author/funder. All rights reserved. No reuse allowed without permission.

block resistance mechanisms (*11*). Consistent with these obstacles, palbociclib has shown limited anti-tumor activity followed by recurrence in a genetic model of diffuse, intrinsic pontine glioma (*12*), and in patient-derived xenograft (PDX) mouse models of medulloblastoma (*1*, *2*). Palbociclib was ineffective as a monotherapy in Phase II clinical trials for recurrent glioblastoma patients with detectable RB expression (NCT01227434) (*13*). Dose-limiting toxicities may have contributed to poor clinical efficacy, as the tested doses were low relative to doses in preclinical studies and many patients required dose reductions due to neutropenia. At the doses that were tolerable for patients, no pharmacodynamic (PD) effect was noted and all patients recurred during therapy (*13*).

Therefore, addressing CNS drug delivery and mechanisms of resistance are needed in order to realize the potential of palbociclib for medulloblastoma, and more broadly for brain tumor therapy.

We have previously shown that polyoxazoline (POx) based amphiphilic block copolymer micelles can act as nanoparticle carriers of diverse small molecules for CNS delivery (*14*, *15*). POx delivery of the SHH inhibitor vismodegib increases brain and tumor drug exposure, reduces systemic toxicity and providing increased efficacy (*16*). Based on these prior studies, we tested whether POx delivery improved palbociclib efficacy. We have designed a novel POx block copolymer to effectively load palbociclib. The new polymer formed charge-charge and hydrophobic interactions with palbociclib resulting in formation of small uniform nanoparticles which release the drug in sustained manner over time. We generated mice with SHH subgroup medulloblastoma by breeding *hGFAP-Cre* mice that express Cre recombinase in CNS stem cells during development with *SmoM2* mice that express a Cre-conditional oncogenic allele of *Smo*. The resulting *G-Smo* mice developed medulloblastoma with 100% penetrance by P10 and,

bioRxiv preprint doi: https://doi.org/10.1101/2021.06.09.447757; this version posted June 9, 2021. The copyright holder for this preprint (which was not certified by peer review) is the author/funder. All rights reserved. No reuse allowed without permission.

untreated, died of progressive tumors by P20, as in prior studies (*16-19*). Consistent with the previously reported data, oral dosing or systemic dosing of free palbociclib (Palbo-HCl) didn't induce survival benefits. Next, we subjected *G-Smo* mice to treatment with formulation of palbociclib loaded into POx micelles (POx-Palbo) and analyzed pharmacokinetics, pharmacodynamics, toxicity and efficacy and compared to systemically delivered Palbo-HCl. To identify potential targets for combinational therapy, we investigated the effects of chronic CDK4/6 inhibition using immunofluorescence and single-cell RNA-seq (scRNA-seq). In parallel, we tested the potential of agents targeting SHH signaling or DNA replication to limit resistance when combined with palbociclib Our results show that POx delivery improved the CNS PK and efficacy of palbociclib, identify palbociclib-induced changes in gene expression in the tumors cells that proliferated during therapy, and show that combining POx-Palbo with the mTOR inhibitor sapanisertib dramatically increased efficacy compared to either agent alone.

RESULTS

Block copolymer design altered the loading of palbociclib into POx nanoparticles

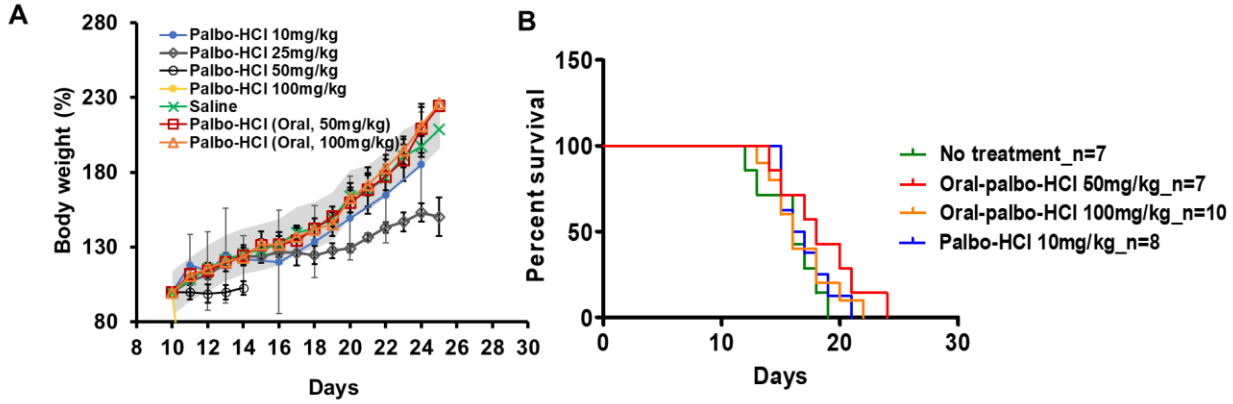

Fig. 1. (A) Maximal Tolerated Dose (MTD) of Palbo-HCl following oral or systemic administration. The weights of mice treated with the indicated formulations were recorded over time. The gray range indicates the mean weights of ± SEM of littermate controls. (B) Kaplan-

bioRxiv preprint doi: https://doi.org/10.1101/2021.06.09.447757; this version posted June 9, 2021. The copyright holder for this preprint (which was not certified by peer review) is the author/funder. All rights reserved. No reuse allowed without permission.

Meir curve of Palbo-HCl following oral or systemic administration in *G-Smo* mice. Oral Palbo-HCl was dosed daily starting on postnatal day 10. Palbo-HCl IP was administered on postnatal days 10-14 (P10-14) and then every other day.

Systemic dosing is one of the approaches to increase exposure to the drug. Therefore, we compared the efficacy of conventional Palbo-HCl following systemic versus oral dosing in *G-Smo* mice. To determine Maximal Tolerated Dose (MTD), Palbo-HCl was dissolved in 50mM sodium L-lactate buffer and escalating doses were administered into healthy, non-tumor bearing pups by oral gavage or intraperitoneal (IP) injection. We weighed the mice daily and compared their weight gain to saline-treated littermate controls. The MTD was defined as the highest dose that did not reduce weight gain by >15%. The MTD of Palbo-HCl IP was 100 mg/kg orally and 10 mg/kg IP **(Fig. 1A)**. Next, we evaluated the effect of Palbo-HCl in medulloblastoma-bearing *G-Smo* mice. The mice were dosed at MTD dose and dosing schedule. No statistical differences were found between saline and Palbo-HCl treated groups, administered either orally or IP, indicating that orally dosed Palbo-HCl is not effective in *G-Smo* mice and can't be dosed systemically due to toxicity and lack of efficacy indicating ultimate need in drug formulation for systemic administration **(Fig. 1B)**.

We first attempted to load palbociclib into the POx-A, hydrophilic, non-charged A-B-A type copolymer, (P[$MeOx_{34}$-*b*-$BuOx_{20}$-*b*-$MeOx_{35}$] (M_n = 8.6 kg/mol)) that we previously used to formulate vismodegib (*16*). However, the loading capacity of palbociclib in POx-A was very low **(Fig. 2A)**. Palbociclib is a pyridopyrimidine and forms hydrophobic as well as hydrogen bonds due to its secondary piperazine nitrogen (pK_a 7.4) and pyridine nitrogen (pK_a 3.9) groups which act as hydrogen donor/acceptors. Thus, we optimized the loading of palbociclib into micelles by designing new POx block co-polymers with stronger polymer-drug interactions based on physico-chemical properties of palbociclib. We synthesized three different copolymers with

bioRxiv preprint doi: https://doi.org/10.1101/2021.06.09.447757; this version posted June 9, 2021. The copyright holder for this preprint (which was not certified by peer review) is the author/funder. All rights reserved. No reuse allowed without permission.

carboxylic groups on the side chains and varying hydrophobicity: POx-B: hydrophilic A-B-A type copolymer (P[$MeOx_{38}$-*b*-$PpaOx_{27}$-*b*-$MeOx_{38}$], M_n = 10.6 kg/mol), POx-C: an A-B-C copolymer, (P[$MeOx_{33}$-*b*-$BuOx_{21}$-*b*-$PpaOx_{29}$], M_n = 9.9 kg/mol) with hydrophilic methyl and hydrophobic butyl groups, and the most hydrophobic POx-D: A-B-C copolymer with hydrophobic ethyl and butyl blocks, (P[P[$EtOx_{34}$-*b*-$BuOx_{21}$-*b*-$PpaOX_{31}$], M_n = 10.7 kg/mol) **(fig. S1)**. We then assessed the ability of each polymer to encapsulate palbociclib using the thin film method.

Introducing carboxylic groups alone, as in POx-B, was not sufficient to improve drug loading. Adding hydrophobic blocks, as in POx-C and POx-D, effectively improved drug loading to ~28% LC. The further increase in hydrophobicity in POx-D compared to POx-C, reduced the particles size and size distribution (**Fig. 2B**). The POx-D-palbociclib micelles were small, spherical particles with mean size of 55nm and narrow size distribution (PDI < 0.1) as determined by dynamic light scattering (DLS) and transmission electron microscopy (TEM; **Fig. 2C).** We selected the POx-D formulation as optimal based on loading capacity and particle size and designated it as POx-Palbo for further studies. *In vitro* release studies of POx-Palbo showed a sustained release profile without burst release, with approximately 30% of palbociclib released in 6 hours and 90% released within 48 hours **(Fig. 2D)**.

bioRxiv preprint doi: https://doi.org/10.1101/2021.06.09.447757; this version posted June 9, 2021. The copyright holder for this preprint (which was not certified by peer review) is the author/funder. All rights reserved. No reuse allowed without permission.

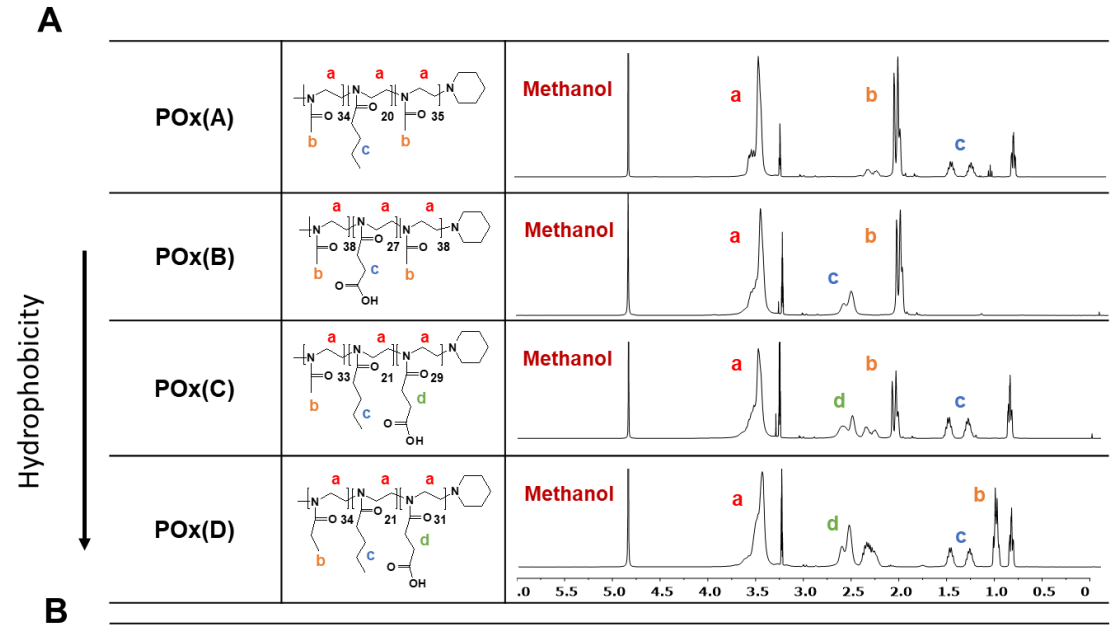

B

Polymer	Size (nm)	PDI	Loading capacity (%)	Loading efficiency (%)
POx(A)/Palbociclib	132.8±14.9	0.25±0.03	3.4±0.5	11.9±1.4
POx(B)/Palbociclib	517.8±66.5	0.66±0.13	6.2±1.3	16.6±3.8
POx(C)/Palbociclib	176.4±3.0	0.20±0.03	27.5±2.1	95.0±10.0
POx(D)/Palbociclib	55.2±1.4	0.07±0.03	27.7±0.4	97±1.2

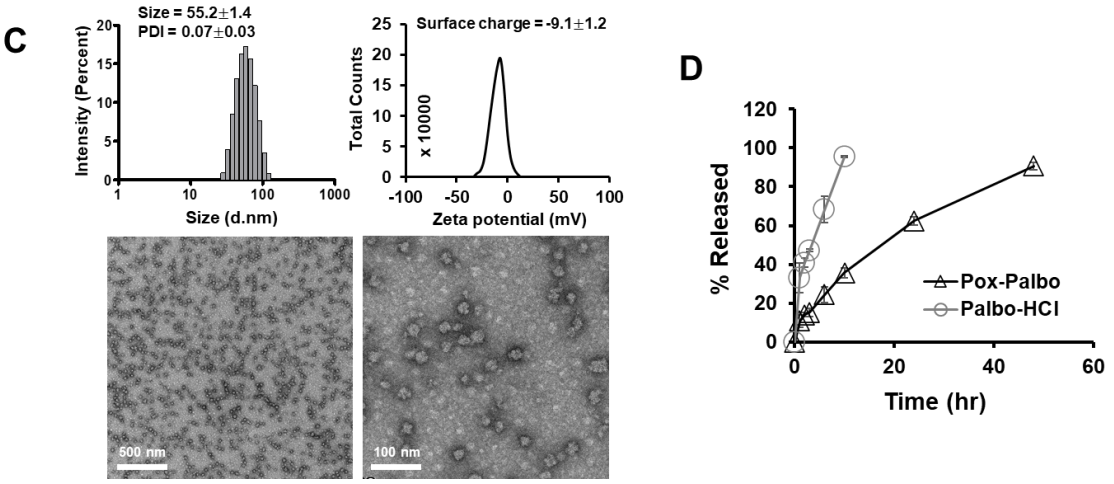

Fig. 2. (A) Strucutres of poly(2-oxazoline) triblock copolymers. The structures were cofirmed by ^{1}H NMR spectrum (in MeOD) by indenfying NMR peaks. (B) Particle size, size distribution and loading parameters (LC%, LE%) of POx-Palbo micelles prepared from indicated polymers. Loading capacity (%) = M_{drug} / (M_{drug} + $M_{excipient}$) × 100 %, Loading efficiency (%) = M_{drug}/ ($M_{drug\ added}$) × 100 % (n = 3 ± SD). (C) Particle size distribution (z-average, Dz, by DLS), Zeta potential and morphology (by TEM, scale bar = 500 nm (left), 10 nm (right)). (D) Palbociclib release profile from POx-Palbo incubated in 10% fetal bovine serum (FBS) solution at 37℃ over time. Palbo-HCl was used as penetration control.

bioRxiv preprint doi: https://doi.org/10.1101/2021.06.09.447757; this version posted June 9, 2021. The copyright holder for this preprint (which was not certified by peer review) is the author/funder. All rights reserved. No reuse allowed without permission.

POx micelle formulation decreased systemic toxicity.

To compare the tolerability of POx-Palbo versus Palbo-HCl, we determined the MTD of POx-Palbo. We injected healthy, non-tumor bearing pups intraperitoneally with escalating doses of POx-Palbo daily on postnatal days 10-14 (P10-14) and then every other day until P26. We weighed the mice each day and compared their weight gain to saline-treated littermate controls. The MTD for POx-Palbo was 50 mg/kg (**Fig. 3A**) versus 10 mg/kg for Palbo-HCl and POx-Palbo showed superior tolerability in parenteral administration.

Next, we exposed mice 25 mg/kg of Palbo-HCl or POx-Palbo daily on postnatal days 10-14 (P10-14) and then every other day until P24. Complete blood counts (CBC) or blood chemistry including serum levels of liver enzymes, total protein, albumin, blood urea nitrogen and creatinine were comparable to saline-treated controls (**Fig. 3B**). We also examined the histology of major organs (Heart, thymus, lung, liver, spleen, and kidney). All mice in Palbo-HCl treated group showed chronic fibrosis and capsules formation in several organs as well as the peritoneal lining. There was also a mild on-going inflammation in these fibrotic lesions suggesting continuing irritation. However, the POx-Palbo treated mice showed none of these toxicities, suggesting that POx-Palbo is not released in the peritoneal cavity but absorbed into circulation reaffirming the advantage of drug retention in polymeric micelles **(Fig. 3C).**

bioRxiv preprint doi: https://doi.org/10.1101/2021.06.09.447757; this version posted June 9, 2021. The copyright holder for this preprint (which was not certified by peer review) is the author/funder. All rights reserved. No reuse allowed without permission.

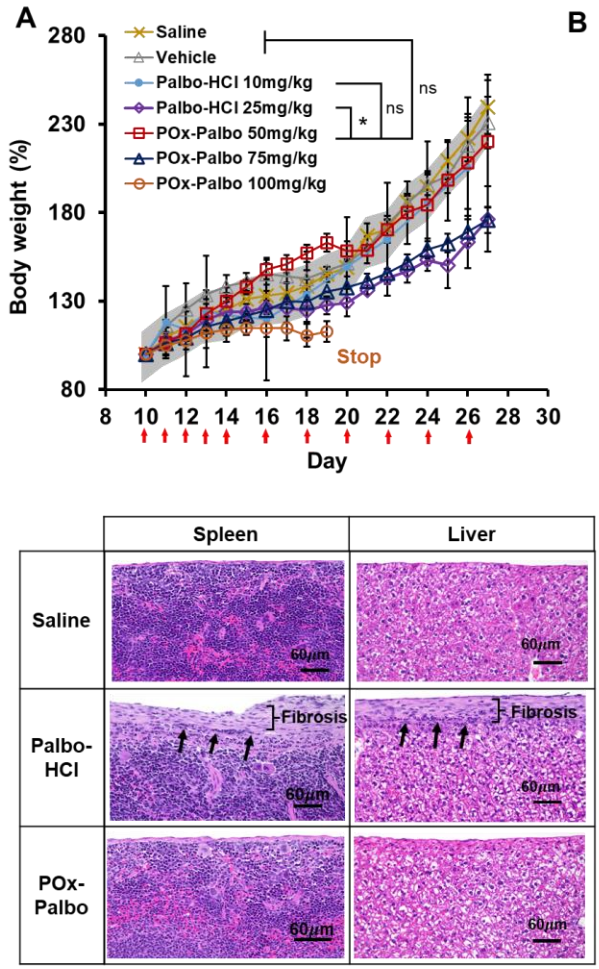

B

		Saline	Palbo-HCl	POx-Palbo	Normal range
Complete blood count	RBC	7.9±0.2	7.5±0.2	7.8±0.3	7~12
	WBC	3.7±1.2	3.6±1.3	3.8±0.8	1.8~5.2
	PLT	341±60	616±76	650±263	285~890
	Neutro	16.8±1.8	24.5±5.6	21.5±3.3	8~48
	Mon	3.2±0.2	5.3±1.5	5±1.9	0~7
	Lym	80.4±1.7	70.2±6.2	73.5±4.2	57~93
Blood chemistry	ALT	35.7±6.5	39.7±4.0	47±4.7	42~73
	AST	97±17	86±5	127±20	51~122
	T.P	4.9±0.2	4.6±1.0	4.9±0.2	4.4~5.8
	Albumin	3.0±0.2	2.8±0.1	2.9±0.2	1.4~3.1
	BUN	21.3±2.1	18.2±5.8	21.2±5.5	19-32.2
	Cr	0.42±0.04	0.39±0.05	0.26±0.07	0.2~0.9

RBC; Red blood cell (number of cells 10^{12}/L), WBC; White blood cell (number of cells 10^{9}/L), PLT; Platelet (count 10^{9}/L) Neutro; Neutrophil (% in WBC), Mono; Monocyte (% in WBC), Lymphs; Lymphocyte (% in WBC), ALT; Alanine aminotranferease (U/L), AST; aspartate aminotransferase (U/L), T.P; Total protein (g/dL), Albumin (g/dL), BUN; Blood urea nitrogen (mg/dL), Cr; Creatinine (mg/dL)

Fig. 3. POx-Palbo reduces toxicity. (A) The weights of mice treated with the indicated formulations over time. The gray range indicates the mean weights of ± SEM of littermate controls (*$p < 0.05$). (B) Complete blood count and clinical chemistry parameters and (C) Hemotoxylin & eosin (H&E) staining of C57BL/6 mice treated with saline, Palbo-HCl, or POx-Palbo (equivalent palbociclib 25 mg/kg). The square bracket and arrows indicate the fibrosis and ongoing inflammatory cells respectively. Mice were treated IP daily on postnatal days 10-14 (P10-14) and then every other day until P24, and blood samples and tissues were collected 24h after the last injection (P25) (n = 3 ± SD).

POx micelles improved palbociclib delivery to the brain and brain tumors

We compared the pharmacokinetics of Palbo-HCl and POx-Palbo in the blood, forebrain and medulloblastomas of *G-Smo* mice. For these comparisons, we administered each formulation at a constant palbociclib dose of 25 mg/kg, selected as the highest IP dose of Palbo-HCl that did not produce fatal toxicity. We incorporated tritiated palbociclib into POx-Palbo and Palbo-HCl

bioRxiv preprint doi: https://doi.org/10.1101/2021.06.09.447757; this version posted June 9, 2021. The copyright holder for this preprint (which was not certified by peer review) is the author/funder. All rights reserved. No reuse allowed without permission.

formulations administered these tritium-labeled agents to groups of replicate *G-Smo* mice on P10. We then harvested the mice at successive time points after administration and collected plasma and tissue samples. We measured palbociclib concentrations by scintillation counting and analyzed the results using Phoenix Modeling software.

Palbo-HCl showed shorter times to peak drug concentrations (T_{max}) in plasma and all tissues sampled, and higher volume of distribution (8.45 mL compared to 3.07 mL for POx-Palbo (p-value <0.05). While C_{max} in plasma was comparable between the formulations, the C_{max} of POx-Palbo in the tumor was 75% higher (5.45 μg/g compared to 3.28 μg/g) and the AUC in the tumor was nearly two-fold greater (p-value <0.05) (**Fig. 4 A and B**). Palbo-HCl produced higher concentrations in the kidneys consistent with renal clearance, while POx-Palbo reached higher peak concentrations in the liver concentrations **(table S1),** consistent with typical nanoparticles clearance in the hepatobiliary system (*20*). Compartment modelling highlighted the differences between the free drug and micellar formulation. Palbo-HCl fit a two-compartment model while the POx-Palbo micelles better fit a one compartment model. The additional compartment in the modeling of the Palbo-HCl formulation suggests exposure of additional tissues to palbociclib.

bioRxiv preprint doi: https://doi.org/10.1101/2021.06.09.447757; this version posted June 9, 2021. The copyright holder for this preprint (which was not certified by peer review) is the author/funder. All rights reserved. No reuse allowed without permission.

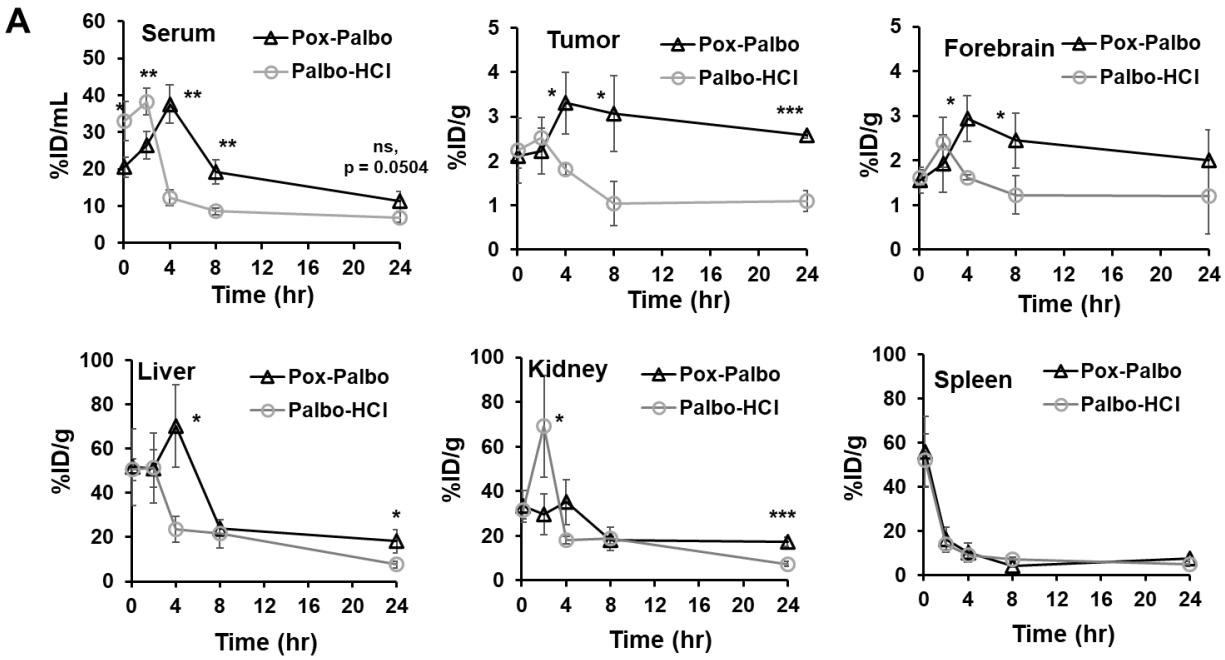

B

	POx-palbo			Palbo-HCl		
	Serum	Tumor	Forebrain	Serum	Tumor	Forebrain
T_{max} (hr) (%ID/ml)	4	4	4	2	2	2
C_{max} (μg/ml or μg/g)	52.83	5.45 *	4.3 *	49.04	3.28	2.84
AUC_{last} (h× μg/mL)	706.68 *	104.10 *	83.37 *	380.90	45.09	46.3
Vd (mL)	3.07 *	-	-	8.45	-	-
CL(mL/hr)	0.15	-	-	0.14	-	-

Fig. 4. Pharmacokinetic profile of POx-Palbo and Palbo-HCl in medulloblastoma-bearing *G-Smo* mice. (A) Plots of palbociclib concentration in serum and major organs (Tumor, forebrain, liver, kidney and spleen over time). (B) PK parametes of given formulations in serum, tumor and forebrain (n = 3 ± SD). Statistical analysis was performed with t-tests, *$p < 0.05$, **$p < 0.01$, ***$p < 0.001$.

bioRxiv preprint doi: https://doi.org/10.1101/2021.06.09.447757; this version posted June 9, 2021. The copyright holder for this preprint (which was not certified by peer review) is the author/funder. All rights reserved. No reuse allowed without permission.

POx-Palbo shows a significant anti-tumor effect, consistently limited by recurrence

We determined the *in vivo* efficacy of POx-Palbo for medulloblastoma therapy by treating *G-Smo* mice, starting at P10, with regimens of 50 mg/kg IP daily (the MTD), 25 mg/kg IP daily (50% of MTD), or 25 mg/kg IP daily for 7 days, followed by 12.5 mg/kg thereafter (**Table s2**). The lower dose POx-Palbo regimens were used to determine if less intense, less toxic doses would differently effect animal survival. We compared survival of mice treated on these regimens to *G-Smo* treated saline as sham controls or treated with Palbo-HCl at the MTD of 10 mg/kg IP daily. All POx-Palbo regimens showed similar efficacy, with increased animal survival and reduced tumor sizes by day P15 (**Fig. 5 A and B**), but all regimens were limited by recurrence during therapy, indicating that efficacy waned over time. To gain insight into the mechanisms that decreased the anti-tumor effect during treatment, we analyzed POx-Palbo pharmacodynamics, and whether the pharmacodynamics changed over the course of therapy.

POx-Palbo pharmacodynamics remain stable as efficacy decreases

We determined pharmacodynamics after *in vivo* POx-Palbo treatment by quantifying RB phosphorylation and cell cycle progression. We administered POx-Palbo IP to *G-Smo* mice, then harvested tumors at defined intervals after drug administration, injecting EdU IP 30 minutes before harvest to label cells at S-phase. We then dissociated the tumors, fixed and stained the cells for pRB, EdU and DNA content, and used flow cytometry to quantify cells at each phase of the cell cycle. We identified the G_0 cells as pRB- population with 2N DNA content, G_1 as the pRB+/EdU- population with 2N DNA content, S-phase as the EdU+/pRB+ population, and G_2/M as the EdU- population with 4N DNA content **(fig. S2**). The fraction of pRB+ cells with 2N DNA content, which included cells in G_1 and early S-phases, was markedly reduced in POx-

bioRxiv preprint doi: https://doi.org/10.1101/2021.06.09.447757; this version posted June 9, 2021. The copyright holder for this preprint (which was not certified by peer review) is the author/funder. All rights reserved. No reuse allowed without permission.

Palbo-treated tumors at both 2 and 6 hours after administration **(Fig. 5 C and D),** demonstrating effective inhibition of the initial phosphorylation of RB by CDK4/6, as expected. This pharmacodynamic effect waned by 24 hours, when pRB+ cells with 2N DNA remained significantly lower compared to controls, but significantly higher compared to 6 hours after administration (**Fig. 5D**). Increasing the dose of POx-Palbo from 25 mg/kg to 50 mg/kg did not increase pRB suppression (**Fig. 5D**), indicating that the dose of 25 mg/kg saturated the capacity of the system to respond to the drug.

Quantifying cells at each phase of the cell cycle (**Fig. 5 E and F)** showed that cell cycling initially decreased after POx-Palbo administration, and then resumed by 24 hours. POx-Palbo-treated tumors showed significantly reduced cells at G1 at 2 hours after injection, and reduced cells at S-phase at 6 hours after injection, indicating reduced progression from G0-S phases (**Fig. 5F**). However, by 24 hours, POx-Palbo-treated tumors showed significantly increased G_1, S and G_2/M cells, indicating a compensatory increase in cell cycling (**Fig. 5F**). In both the pRB and cell cycle studies, POx-Palbo pharmacodynamic effects showed a time dependent decrease over 24 hours that was out of proportion to the smaller time-dependent decrease in drug concentration and therefore could not be explained by pharmacokinetics alone.

To determine if tumors sensitivity to palbociclib was affected by repeated exposure, we treated mice with daily POx-Palbo 25 mg/kg IP for 5 days and then harvested replicate tumors at successive intervals after the fifth dose and analyzed pharmacodynamics using our flow cytometry methods. We found that medulloblastomas treated for 5 days with daily POx-Palbo showed similar temporal patterns of pRB suppression after the fifth dose, indicating that the magnitude and duration of CDK4/6 inhibition were not changed by treatment over this period

bioRxiv preprint doi: https://doi.org/10.1101/2021.06.09.447757; this version posted June 9, 2021. The copyright holder for this preprint (which was not certified by peer review) is the author/funder. All rights reserved. No reuse allowed without permission.

(Fig. 5G). Repeated dosing of POx-Palbo therefore produced a cycle of transient pRB suppression.

Longitudinal studies of tumor growth during therapy showed that this cyclic pRB suppression produced diminishing growth suppression. We measured SHH signaling proliferative capacity in tumors non-invasively *in vivo* by engineering mice to develop medulloblastomas detectable by bioluminescence imaging (BLI). We generated mice with luciferase-expressing tumors by crossing breeders for *G-Smo* mice with *Gli-luc* transgenic mice that report SHH activity through a GLI-sensitive luciferase reporter transgene (*21*), as in our prior studies (*22*). The resulting *G-Smo*$^{Gli\text{-}luc}$ mice developed medulloblastomas with BLI signal that increased progressively from P10-P14 (**Fig. 5H, control**). Daily treatment of replicate *G-Smo*$^{Gli\text{-}luc}$ mice with POx-Palbo 25 mg/kg IP produced an initial decrease in mean BLI, indicating reduced tumor progression. By day 4, however, BLI signal began increasing, indicating that tumor growth resumed while on daily therapy **(Fig. 5H)**. Tumor growth therefore resumed during the period of stable pharmacodynamics, indicating that the recurrence did not require resistance to pRB suppression, but rather a dissociation between pRB suppression and growth suppression. To define the processes that allow medulloblastoma cells to proliferate during ongoing palbociclib treatment, we compared the tanscriptomic profiles of proliferative medulloblasted cells in untreated *G-Smo* tumors versus tumors in *G-Smo* mice on POx-Palbo therapy, using scRNA-seq.

bioRxiv preprint doi: https://doi.org/10.1101/2021.06.09.447757; this version posted June 9, 2021. The copyright holder for this preprint (which was not certified by peer review) is the author/funder. All rights reserved. No reuse allowed without permission.

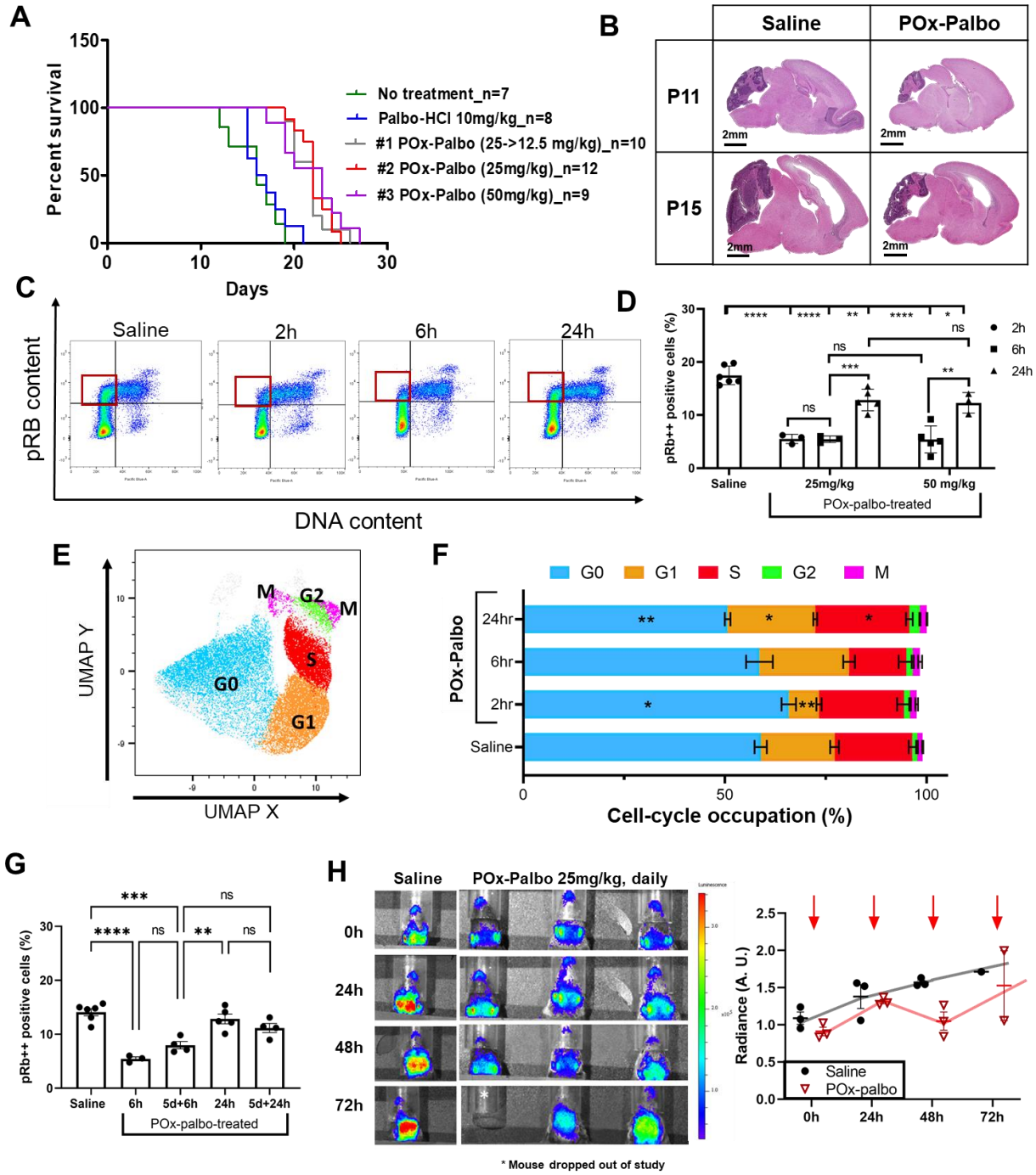

Fig. 5. Pharmacodynamic analysis of POx-Palbo in medulloblastoma- bearing *G-Smo* mice. (A) Kaplan-meir curve of POx-Palbo treatments (#1-3) and palbo-HCl in *G-Smo* mice. (B) H&E of POx-Palbo treated brains at 24 hours (P11) and 5 daily treatments (P15) compared to saline controls. (C) Two-dimensional flow cytometry analysis of DNA content (x-axis) and pRB content (y- axis) in POx-Palbo treated (2-24h) *G-Smo* mice. (D) Quantification of highly phosphorylated cells in G1 (Red square) in POx-Palbo-treated mice. Statistics performed with One-way ANOVA. (E) UMAP qualitative map of tumor cells dissociated from *G-Smo* mice. (F)

bioRxiv preprint doi: https://doi.org/10.1101/2021.06.09.447757; this version posted June 9, 2021. The copyright holder for this preprint (which was not certified by peer review) is the author/funder. All rights reserved. No reuse allowed without permission.

Cell-cycle occupation analysis of 25 mg/kg of POx-Palbo treated (2-24h) *G-Smo* mice. Unpaired t-test of each cell-cycle phase compared to saline control. (G) Quantification of highly-phosphorylated cells in G1 in 25 mg/kg of POx-Palbo treated mice after 5 days. Statistical analysis was performed with One-way ANOVA. (H) Longitdunial dynamic tracing of POx-Palbo in luciferase-tumor bearing mice. Quantified in the right panel. *$p < 0.05$, **$p < 0.01$, ***$p < 0.001$, ****$p < 0.0001$.

scRNA-seq studies identify reduced ribosomal gene expression as a consistent effect of chronic palbociclib therapy

We used Drop-seq (*23*) methods to compare tumors isolated from three P15 *G-Smo* mice treated with 25 mg/kg POx-Palbo daily IP for 5 days to tumors from five age-matched, untreated *G-Smo* mice, as in our prior studies (*17, 22*). Briefly, tumors were harvested, dissociated and individual cells were paired with barcoded, oligo dT-coated beads using microfluidic methods, and bar-coded cDNA was synthesized on the beads. We then prepared and sequenced amplified libraries from the pooled cDNA and used cell-specific bar codes to identify the transcriptome of individual cells in the resulting sequence data. We filtered cells identified by bead-specific barcodes to address unintentional cell-cell multiplexing and premature cell lysis (*24, 25*). 1530 out of 4959 cells from POx-Palbo treated tumors, and 8699 out of 16489 cells from control tumors met criteria and were included in the analysis. To compare the two groups at similar sequencing depths, we randomly down-sampled the control transcript counts to 20% of the original depth (*26*).

We performed an integrated analysis of scRNA-seq data form POx-Palbo treated and control tumors using PCA as in our prior studies (*22*), and generated 2-dimensional UMAP projection in which individual cells were placed according to their similarities, forming clusters of like cells **(Fig. 6A)**. As in our prior medulloblastoma scRNA-seq studies, cells grouped in either discrete clusters or in a set of clusters with shared borders. We identified each cluster

bioRxiv preprint doi: https://doi.org/10.1101/2021.06.09.447757; this version posted June 9, 2021. The copyright holder for this preprint (which was not certified by peer review) is the author/funder. All rights reserved. No reuse allowed without permission.

using stromal cell markers and the CGNP lineage marker, as validated in our prior medulloblastoma scRNA-seq studies (*17, 22*). These markers showed that each discrete cluster comprised a different type of stromal cells typical of brain tissue including astrocytes, oligodendrocytes, myeloid cells, endothelial cells and fibroblasts and the 6 clusters in the multi-cluster complex as medulloblastoma cells **(Fig. 6 A and B; Table 1)**. The expression patterns of proliferation markers *Mki67* and *Pcna*, and *Gli1*, a key effector of SHH-driven proliferation identified the cells of clusters 0,1,3 and 5 as proliferative; similarly intermediate differentiation markers *NeuroD1* and *Cntn2*, and late differentiation markers *Grin2b* and *Gria2*, placed the cells of clusters 2 and 4 in successive states of differentiation **(Fig. 6 C and D).** Together these markers defined a spectrum with opposite proliferative and differentiated poles **(Fig. 6 C and D)**.

Disaggregating the data by treatment group showed that medulloblastoma cells were not evenly distributed in the tumor cell clusters **(Fig. 6 E and F)**. Palbociclib-treated tumors contained significantly larger fractions of cells in cluster 4 (p=0.023), the most differentiated cluster. Among proliferative medulloblastoma cells, cluster 5 comprised almost exclusively palbociclib-treated cells (p=0.024, Wilcoxon rank sum test), cluster 0 comprised predominantly control cells (p=0.024), and clusters 1,3 showed similar populations from both treatment groups. POx-Palbo-treated tumors thus contained both more differentiated tumor cells, consistent with drug-induced growth-suppression, and a distinct population of proliferating cells with a transcriptomic profile that was different from proliferating cells in control tumors.

bioRxiv preprint doi: https://doi.org/10.1101/2021.06.09.447757; this version posted June 9, 2021. The copyright holder for this preprint (which was not certified by peer review) is the author/funder. All rights reserved. No reuse allowed without permission.

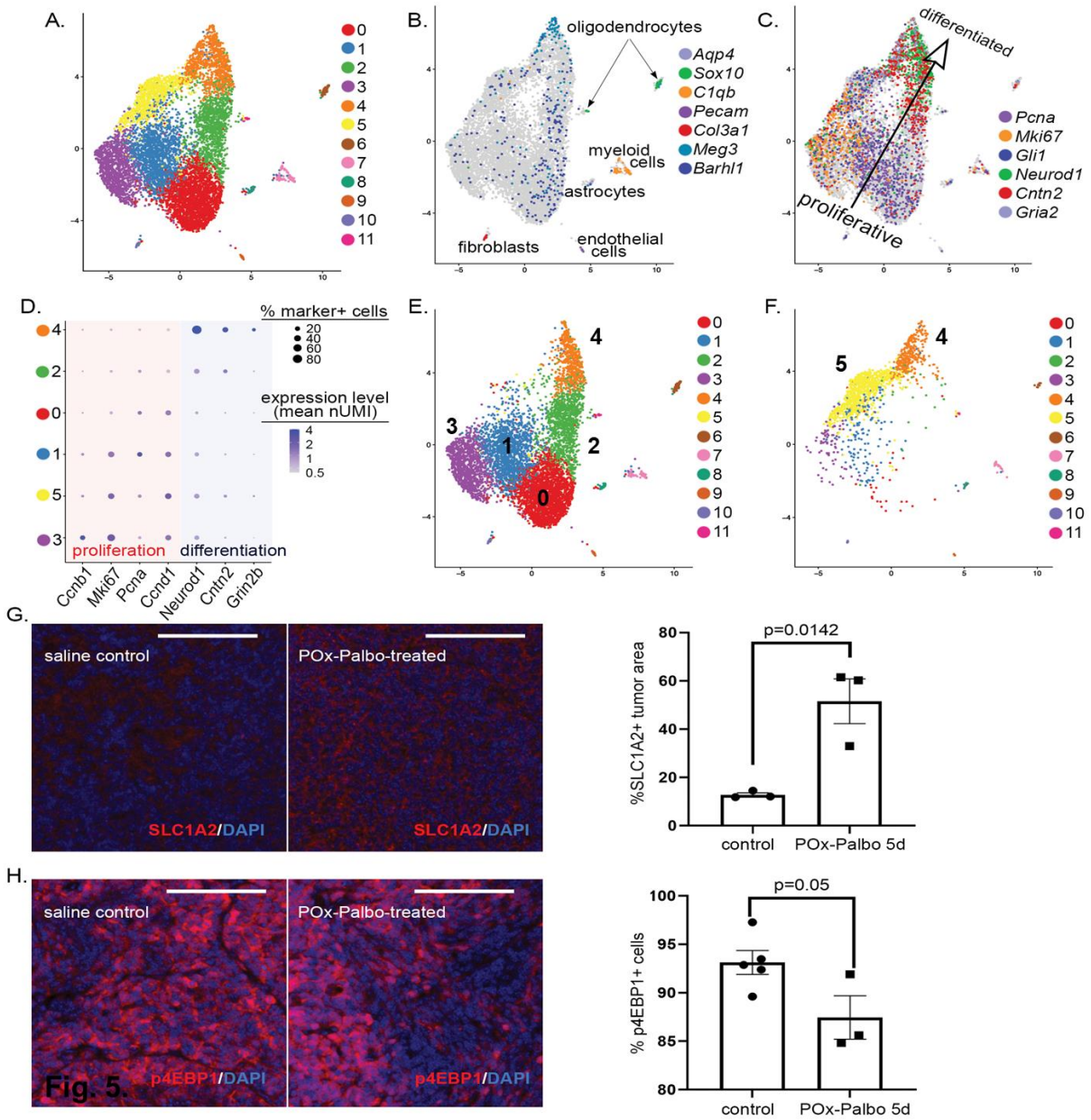

Fig. 6. scRNA-seq shows key differences in the composition of POx-Palbo-treated tumors, including a population of proliferative medulloblastoma cells not found in control tumors, marked by up-regulation of SLC1A2 and down-regulation of mTORC1 activity. (A) UMAP projection of all cells from POx-Palbo treated and control tumors, grouped by transcriptomic similarities into color-coded clusters. (B) Expression of indicated markers is color-coded onto the UMAP projection from (A), with stromal cluster identities indicated. (C) Expression of proliferation and differentiation markers is color-coded onto the UMAP projection from (A). The arrow indicates the overall direction of progression from the proliferative to the differentiated pole. (D) Dot Plot shows the magnitude and frequency of the expression of indicated proliferation and differentiation markers in the indicated tumor cell clusters. (E,F) UMAP from

bioRxiv preprint doi: https://doi.org/10.1101/2021.06.09.447757; this version posted June 9, 2021. The copyright holder for this preprint (which was not certified by peer review) is the author/funder. All rights reserved. No reuse allowed without permission.

(A), disaggregated by condition to show (E) cells from control tumors and (F) cells from POx-Palbo-treated tumors. (G) Representative sections of control and POx-Palbo treated *G-Smo* tumors, immunostained for SLC1A2, with quantification. (H) Representative sections of control and POx-Palbo-treated *G-Smo* tumors, immunostained for p4EBP1, with quantification. P values in (G,H) determined by student's t-test. Scale bars = 100 µm.

Table 1. Cluster identities, markers, and population differences by condition.

Cluster #	Best marker	Designation	Population differences
0	Rpl37, Barhl1	Proliferative tumor cells, high ribosomal genes	Depleted in POx-Palbo-treated p=0.024
1	Mik67, Barhl1	Proliferative tumor cells	
2	Tubb3, Barhl1	Early differentiating tumor cells	
3	Ccnb1, Barhl1	Mitotic tumor cells	
4	Neurod1, Meg3	Late differentiating tumor cells & neurons	Enriched in POx-Palbo-treated p=0.023
5	Slc1a2, Barhl1	Proliferating tumor cells	Enriched in POx-Palbo-treated p=0.024
6	Olig1	Early oligodendrocytes	
7	C1qa	Myeloid	
8	Aqp4	Astrocytes	
9	Cldn5	Endothelial	
10	Dcn	Fibroblasts	
11	Mag, Mog	Late oligodendrocytes	

We considered that the gene expression patterns that distinguished cluster 5 cells from the other proliferative cells may include both potentially growth-suppressive mechanisms that failed to block proliferation and resistance mechanisms that allowed proliferation to continue on therapy. To resolve the differential gene expression pattern specific to cells proliferating during POx-Palbo treatment, we identified genes differentially expressed in cluster 5 cells, compared to the cells of clusters 0,1 and 3, the proliferative cells that were either control-specific or found in both genotypes and then filtered to include only the set of genes that was expressed by a 2-fold or greater proportion of cluster 5 cells, or the set expressed by a 2-fold or greater proportion of cells of clusters 0, 1, and 3 **(Data file S1)**. We subjected both sets to Gene Ontology (GO) enrichment analysis to identify biological processes discernably affected.

bioRxiv preprint doi: https://doi.org/10.1101/2021.06.09.447757; this version posted June 9, 2021. The copyright holder for this preprint (which was not certified by peer review) is the author/funder. All rights reserved. No reuse allowed without permission.

GO analysis of the set of genes showing greater expression in clusters 0, 1, and 3 identified translation as the process most strongly enriched ($p=1.2 \times 10^{-39}$), with diverse biosynthetic processes showing enrichment. GO analysis of the set of genes showing greater expression in cluster 5 cells identified less specific terms including "positive regulation of biologic process" and "positive regulation of metabolic process" as the most significantly enriched ($p=6.5 \times 10^{-9}$ and 6.8×10^{-9} respectively), with chromatin organization also significantly affected. Consistent with increased translation in clusters 0, 1, and 3, we noted increased expression of diverse ribosomal genes and *Eef1b2* **(Data file S1)**. Consistent with metabolic and chromatin alterations induced by palbociclib, we noted increased expression of the glutamate transporter *Slc1a2* and the chromatin modifier *Smarca4* in cluster 5 cells **(Data file S1)**. We confirmed increased protein expression of SLC1A2 (aka GLT1) in replicate POx-Palbo treated and control tumors using immunohistochemistry (IHC) **(Fig. 6 G)**.

Signaling through mTORC1 regulates ribosomal gene transcription as part of a general regulation of translation (*27*), and we therefore analyzed whether reduced mTORC1 acted as up-stream determinant of the transcriptomic response to chronic palbociclib treatment. Inhibition of mTORC1 also increases SLC1A2 expression in other cell types (*28*), which also suggested reduced mTORC1 activity in POx-Palbo treated medulloblastomas. To investigate mTORC1 activation, directly, we used phosphorylated 4EBP1 (p4EBP1) as a marker of mTORC1 activity. We compared p4EBP1 in replicate *G-Smo* mice treated for 5 days with POx-Palbo versus untreated *G-Smo* controls, using IHC. We found significantly fewer p4EBP1+ cells in POx-Palbo-treated tumors, indicating reduced mTORC1 activation, consistent with decrease in ribosomal genes in the scRNA-seq data **(Fig. 6H)**.

bioRxiv preprint doi: https://doi.org/10.1101/2021.06.09.447757; this version posted June 9, 2021. The copyright holder for this preprint (which was not certified by peer review) is the author/funder. All rights reserved. No reuse allowed without permission.

These data show correlations between palbociclib treatment and both reduced mTORC1 activity and increased SLC1A2 expression, validating our scRNA-seq data. These correlations do not show whether reduced mTORC1 activity or increased SLC1A2 are direct effects of the drug or secondary effects of pRB suppression, or whether the effects are mechanisms of resistance that allows continued proliferation. We hypothesized, however, that whether reduced mTORC1 activity was growth-suppressive or growth-enabling, the mTORC1 activity in POx-Palbo-treated tumors might already be at the lower limit of tolerability for proliferating cells, resulting in increased sensitivity to small molecule mTORC1 inhibitors. We therefore tested whether combining POx-Palbo with the mTORC1 inhibitor sapanisertib, which, like palbociclib shows medulloblastoma efficacy limited by recurrence (*29*), would produce an efficacy greater than either single agent.

Testing combination therapy with POx-Palbo plus multiple agents validated POx-(Palbo+Sapanisertib) and failed to show benefits of other combinations

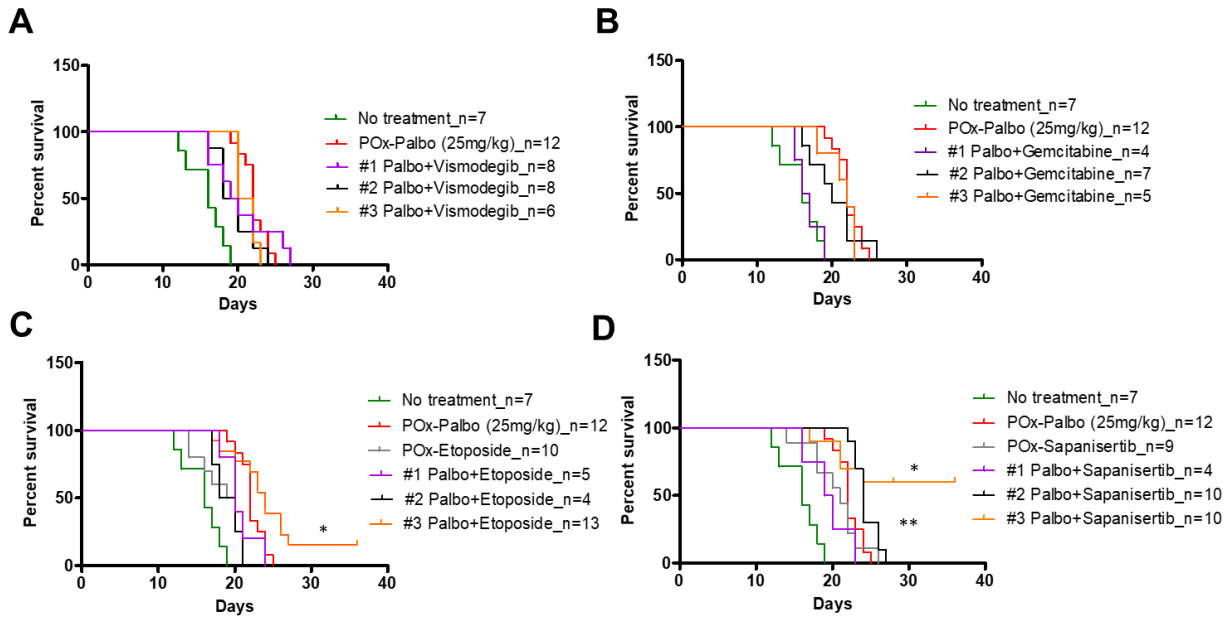

bioRxiv preprint doi: https://doi.org/10.1101/2021.06.09.447757; this version posted June 9, 2021. The copyright holder for this preprint (which was not certified by peer review) is the author/funder. All rights reserved. No reuse allowed without permission.

Fig. 7. Kaplan-Meier survival curves for *G-Smo* mice treated with (A) POx-(Palbo+Vismo) (B) POx-Palbo+Gemcitabine (C) POx-(Palbo+Etop), (D) POx-(Palbo+Sap) at various treatment regimens. Statistical tests performed with Log-rank (Mantel-Cox) Test. P value is obtained by comparing the POx-Palbo and combination. *$p < 0.05$, **$p < 0.01$.

In parallel with the palbociclib-sapanisertib combination, we tested the potential of agents targeting SHH signaling or DNA replication to limit resistance when combined with palbociclib. We theorized that 1) vismodegib, which inhibits the SHH receptor component SMO, would combine favorably with palbociclib by targeting 2 distinct points in the oncogenic SHH signaling pathway, SMO and CDK4/6, which is s downstream effector of SHH-SMO-GLI signaling. 2) replication-targeted agents gemcitabine or etoposide would enhance palbociclib efficacy by addressing tumor cells that progress to S-phase despite CDK4/6 inhibition, and that the compensatory increase in cycling cells 24 hours after palbociclib would increase sensitivity to gemcitabine or etoposide. We tested these hypotheses by developing regimens for each agent, then treating cohorts of *G-Smo* mice with each agent, either as a single agent, or in combination with POx-Palbo. For non-water soluble drugs (vismodegib, etoposide, sapanisertib) we have developed POx based micellar formulation, building upon previous data that loading drugs into POx micelles reduces toxicity and improves efficacy of treatment. Our prior studies showed that vismodegib administered systemically to *G-Smo* mice in polyoxazoline nanoparticles (POx-Vismo) was more effective for medulloblastoma therapy than conventional vismodegib (*16*). We previously developed a formulation of etoposide loaded into POx micelles (POx-Etop) and showed that this formulation was less toxic and more effective than free drug in a mouse lung cancer models (*30, 31*). The formulations were characterized by size, size distribution and drug loading **(fig. S3A).** For gemcitabine studies, we used a conventional, rather than POx formulation, as gemcitabine is water soluble and did not load well into polyoxazoline micelles. The dose of single drug was determined based on MTD evaluations *in vivo*. Studies of the

bioRxiv preprint doi: https://doi.org/10.1101/2021.06.09.447757; this version posted June 9, 2021. The copyright holder for this preprint (which was not certified by peer review) is the author/funder. All rights reserved. No reuse allowed without permission.

growth of healthy mice on escalating regimens of gemcitabine identified 5 mg/kg every three days as the MTD **(fig. S3B)**. The MTD for POx-Etop was 5 mg/kg every 5 days **(fig. S3C)**, however at this dose mice showed marginally acceptable weight gain, and we therefore used 2.5 mg/kg (50% of the MTD) for tumor treatment. The MTD for formulation of sapanisertib loaded into POx micelles (POx-Sap) was 0.2 mg/kg daily **(fig. S3D)**; as with etoposide we used 0.1 mg/kg dosing due to marginal weight gain at the MTD. For combinational studies, we co-encapsulated the two drugs in a single nanoparticle formulation. The drugs ratios were varied to evaluate the effects of drug ratios on treatment outcomes (**fig. S4).**

To combine vismodegib and palbociclib, we administered POx-(Palbo+Vismo) starting at P10 using 3 different treatment schedules, including reducing POx-Palbo to 12.5 mg/kg after 5 doses and increasing Vismo dose to 100 mg/kg **(Table 2; table s3)**. We tested these different regimens to identify the most effective, tolerable combination; none of tested regimens, however, were superior to either POx-Palbo or Pox-Vismo as single agents **(Fig. 7A).** Next, we tested 3 different schedules of combined gemcitabine and POx-Palbo **(Table 2; table s4)** all failed to improve survival compared to Pox-Palbo alone **(Fig. 7B)**.

Treatment of *G-Smo* mice with single agent POx-Etop 2.5 mg/kg IP every 5 days improved survival compared to sham treatment **(p = 0.0298; Fig. 7C)**. For combination therapy, we tested multiple regimens with varied doses of etoposide and palbociclib **(Table 2; table s5)**. The regimen of POx-(Palbo+Etop) (25 mg/kg palbociclib/2.5 mg/kg etoposide) every 5 days starting on P10 and POx-Palbo 25 mg/kg daily in between improved mouse survival relative to POx-Palbo alone (p=0.047) or POx-Etop alone (p=0.001) and was more effective than reducing Palbo dose to 12.5 mg/kg on P15 or starting the treatment with Palbo alone, but recurrence during therapy remained a consistent limitation **(Fig. 7C)**. Combining palbociclib with the

bioRxiv preprint doi: https://doi.org/10.1101/2021.06.09.447757; this version posted June 9, 2021. The copyright holder for this preprint (which was not certified by peer review) is the author/funder. All rights reserved. No reuse allowed without permission.

replication-targeting agent etoposide therefore enhanced efficacy but did not sufficiently reduce recurrence.

Single agent POx-Sap dosed at 0.1 mg/kg IP to *G-Smo* mice significantly improved survival compared to no treatment, but all treated mice developed recurrence **(Fig. 7D)**. For combination therapy, we tested multiple regimens **(Table 2; table s6)**. Regimen 3, there the dose of POx-Palbo was reduced and POx-Palbo was dosed less frequently, while the dose of sapanisertib and the frequency of combination treatment was increased was superior to both POx-Palbo alone (p=0.011) and POx-Sap alone (p=0.006) and importantly reduced recurrence during therapy from 100% to 40% **(Fig. 7D)**. Combining palbociclib with mTORC1 inhibitor sapanisertib was therefore markedly more effective in reducing recurrence during treatment than all other combinations tested.

bioRxiv preprint doi: https://doi.org/10.1101/2021.06.09.447757; this version posted June 9, 2021. The copyright holder for this preprint (which was not certified by peer review) is the author/funder. All rights reserved. No reuse allowed without permission.

Table 2. Regimens used in *in vivo* testing

	Drugs Combination		
	Palbociclib	**+ Vismodegib**	**Median survival**
#1	25 mg/kg daily starting on P10	50 mg/kg P10-12 daily, then QOD	19.5
#2	25 mg/kg P10-14 daily, then QOD	50 mg/kg P10-14 daily, then QOD	19
#3	25 mg/kg P10-13 daily, 12.5mg/kg P14-16 daily, then QOD	100 mg/kg P14-16 daily, then QOD	21
	Palbociclib	**+ Gemcitabine**	
#1	25 mg/kg daily starting on P10	50 mg/kg from P12 Q3D	16.5
#2	25 mg/kg daily starting on P10	25 mg/kg from P14 Q5D	20
#3	25 mg/kg P10-13 daily, then 12.5mg/kg daily	25 mg/kg from P14 Q5D	22
	Palbociclib	**+ Etoposide**	
#1	25 mg/kg daily starting on P10	5 mg/kg from P14 Q5D	20
#2	25 mg/kg P10-14 daily, then 12.5mg/kg daily	2.5 mg/kg from P10 Q5D	19
#3	25 mg/kg daily starting on P10	2.5 mg/kg from P10 Q5D	24
#4	25 mg/kg daily starting on P10	2.5 mg/kg from P14 Q5D	21
	Palbociclib	**+ Sapanisertib**	
#1	25 mg/kg daily starting on P10	0.1 mg/kg daily	19.5
#2	25 mg/kg P10-13 daily, then 12.5mg/kg daily	0.1 mg/kg from P14 daily	24
#3	25 mg/kg P10-13 daily, 12.5mg/kg P14-16 daily, then QOD	0.2 mg/kg P14-16 daily, then QOD	> 35 days

Abbreviations: QOD, every other day; Q3D, every third day; Q5D, every fifth day.

Palbociclib and sapanisertib show enhanced pharmacodynamics

Pharmacodynamic studies showed combining palbociclib and sapanisertib enhanced the mechanistic effects of each agent. We compared the temporal patterns of pRB suppression and p4EBP1 suppression after administration of POx-Palbo, POx-Sap or POx-(Palbo+Sap) using flow cytometry and immunohistochemistry **(Fig. 8)**. 6 hours after administration, POx-Palbo, POx-Sap and POx-(Palbo+Sap) significantly and similarly decreased pRB; however, pRB suppression by POx-(Palbo+Sap) was markedly more durable, remaining significantly reduced compared to controls 24 hours after administration **(Fig. 8A)**. The synergistic reduction of phosphor-RB tumor expression was confirmed again by IHC 24 hours after administration **(Fig. 8 B and C)**.

bioRxiv preprint doi: https://doi.org/10.1101/2021.06.09.447757; this version posted June 9, 2021. The copyright holder for this preprint (which was not certified by peer review) is the author/funder. All rights reserved. No reuse allowed without permission.

Both POx-Sap and POx-(Palbo+Sap) significantly reduced p4EBP1 6 hours after administration, but p4EBP1 suppression by POx-(Palbo+Sap) was more durable and persisted over 24 hours **(Fig. 8 D and E).** The enhanced pharmacodynamic effects of palbociclib and sapanisertib, delivered as POx-(Palbo+Sap) support the increased efficacy of the combination, predicted by the scRNA-seq data and demonstrated by the survival studies.

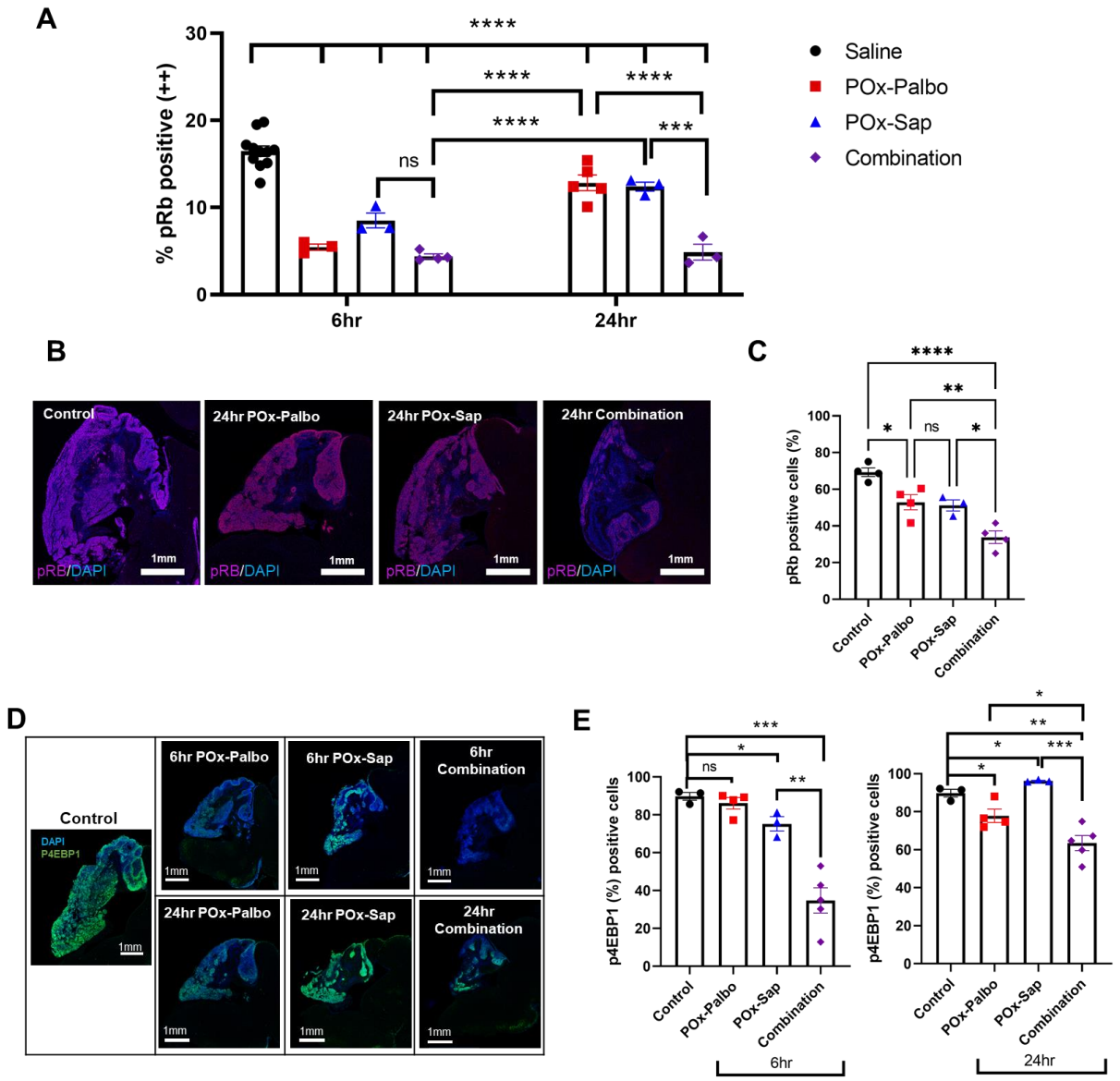

Fig. 8. Pharmacodynamic analysis of POx-(Palbo+Sap) in medulloblastoma-bearing *G-Smo* mice. (A) Quantification of dynamic flow cytometry analysis of highly-phosphorylated G1 cells

bioRxiv preprint doi: https://doi.org/10.1101/2021.06.09.447757; this version posted June 9, 2021. The copyright holder for this preprint (which was not certified by peer review) is the author/funder. All rights reserved. No reuse allowed without permission.

in POx-Palbo (red), POx-sapanisertib (blue), and POx-(Palbo+Sap) (purple) combination in *G-Smo* mice at 6 and 24 hours. Statistical tests performed with One-way ANOVA. (B) Immunofluorescence staining of phospho-RB tumor expression in POx-Palbo, POx-Sap, and POx-(Palbo+Sap) combination at 24 hours. (C) Quantification of phospho-RB tumor expression in treated mice. (D) immunofluorescence staining of phospho-4EBP1 tumor expression in POx-Palbo, POx-Sap, and POx-(Palbo+Sap) combination at 6 and 24 hours. (E) Quantification of phospho-4EBP1 tumor expression in treated mice.Statistical tests performed was t-tests.

DISCUSSION

CDK4/6 inhibitor therapy for brain tumors has been complicated by suboptimal pharmacokinetics and the development of recurrence during therapy. We developed a polyoxazoline micelle-based nanoparticle formulation of the CDK4/6 inhibitor palbociclib, POx-Palbo, which allowed systemic administration of the drug and showed improved CNS pharmacokinetics. Systemic administration of POx-Palbo showed treatment benefit while oral and systemic delivery of Palbo-HCl didn't induce any response, but the efficacy remained limited by recurrence. While pharmacodynamic analysis showed continuous response to palbo, scRNA-seq studies showed specific transcriptional changes in the medulloblastoma cells that remained proliferative during on-going *in vivo* palbociclib treatment, including up-regulation of the glutamate transporter *Slc1a2* and suppression of ribosomal genes downstream of mTORC1 inhibition. mTORC1 inhibition with POx-Sap alone inhibited tumor growth, however, single agent treatment wasn't curative. Targeting both CDK4/6 and mTORC1 by adding sapanisertib to the palbociclib regimen markedly increased anti-tumor efficacy. Similarly enhanced efficacy was not observed on combining palbociclib with vismodegib or gemcitabine; etoposide enhanced the efficacy of palbociclib, but less effectively than sapanisertib despite several dose optimization attempts. These data show the potential for nanoparticle technology to optimize CNS drug

bioRxiv preprint doi: https://doi.org/10.1101/2021.06.09.447757; this version posted June 9, 2021. The copyright holder for this preprint (which was not certified by peer review) is the author/funder. All rights reserved. No reuse allowed without permission.

delivery, and for transcriptomic analysis with single cell resolution to identify processes that when targeted therapeutically can reduce recurrence.

The reduced ribosomal gene expression pattern that we observed in *G-Smo* tumors treated with POx-Palbo *in vivo* matches the patterns of differentially suppressed transcripts previously reported in medulloblastoma cell lines with CDK6 deletion and in *Cdk6*-deleted medulloblastomas that form in *Math1-Cre/SmoM2/Cdk6*$^{-/-}$ mice (*32*). Our data show that this transcriptomic change correlates with decreased mTORC1 activation, demonstrated by reduced p4EBP1. The reduced ribosomal biogenesis in *Cdk6*-deleted SHH medulloblastomas sustains proliferation by inducing production of SMO-stimulating lipids (*32*) and this mechanism may explain the failure of palbociclib to combine well with the SMO inhibitor vismodegib. By inducing SMO-activating lipids through suppression ribosomal function, palbociclib may antagonize vismodegib. In contrast, by reducing mTORC1, which allows medulloblastoma cells to proliferate in the context of reduced CDK4/6 activity, palbociclib increased susceptibility to mTORC1 inhibitors. These data show that when mechanisms of resistance involve downregulation of fundamental biologic processes, such as reduced mTORC1 activity, resistance may be blocked by amplifying rather than inhibiting the resistance mechanism, as in the addition of sapanisertib to palbociclib.

The combination of palbociclib and sapanisertib, suggested by our scRNA-seq and p4EBP1 studies, has been similarly reported to produce enhanced anti-tumor activity in a mouse model of intrahepatic cholangiocarcinoma (ICC) induced by somatic gene transfer of mutant Akt and Yap (*33*). In these ICC tumors, palbociclib alone produces a transient anti-tumor effect, as in *G-Smo* medulloblastoma, in which increased CCND1 promotes resistance. Addition of sapanisertib reduced CCND1 expression and potentiated cell cycle inhibition. In

bioRxiv preprint doi: https://doi.org/10.1101/2021.06.09.447757; this version posted June 9, 2021. The copyright holder for this preprint (which was not certified by peer review) is the author/funder. All rights reserved. No reuse allowed without permission.

medulloblastomas we found that palbociclib resistance did not involve increased CCND1. Sapanisertib, however, potentiated pRB suppression, as in ICC. In both *G-Smo* medulloblastomas and in ICC, single-agent therapy with palbociclib reduced p4EBP1, indicating mTORC1 inhibition, and also potentiated p4EBP1 suppression when combined with sapanisertib (*33*). A potential mechanism for the potentiating effect of palbociclib on sapanisertib-mediated mTORC1 inhibition is suggested by the suppression of CDK4-mediated activation of IRS2 and resulting inactivation of TSC2 (*11*). The mutually enhancing effects of palbociclib and sapanisertib in both SHH medulloblastoma and ICC show that this combination may be effective in diverse cancers driven by different oncogenic pathways in different tissues of origin.

MATERIALS AND METHODS

Materials

All materials for the synthesis of poly(2-oxazoline) block copolymers, methanol, ethanol, and sodium lactate were purchased from Sigma Aldrich (St. Louis, MO). Water and acetonitrile (HPLC grade) were purchased from Fisher Scientific Inc. (Fairlawn, NJ). All materials for the synthesis of poly(2-oxazoline) block copolymers including methyl trifluoromethanesulfonate (MeOTf), 2-methyl-2-oxazoline (MeOx), 2-ethyl-2-oxazoline (EtOx), 2-n-butyl-2-oxazoline (BuOx), and 2-methoxycarboxyethyl-2-oxazoline (MestOx) were dried by refluxing over calcium hydride (CaH_2) under inert nitrogen gas and subsequently distilled prior to use. Palbociclib free base, palbociclib-HCl salt form, vismodegib, etoposide, and gemcitabine were purchased from LC Laboratories (Woburn, MA). Sapanisertib was purchased from Medkoo Biosciences (Morrisville, NC). [^{3}H] Palbociclib was purchased from American Radiolabeled

bioRxiv preprint doi: https://doi.org/10.1101/2021.06.09.447757; this version posted June 9, 2021. The copyright holder for this preprint (which was not certified by peer review) is the author/funder. All rights reserved. No reuse allowed without permission.

Chemicals (St. Louis, MO). Soluene-350 and Ultima Gold LLC scintillation cocktail were purchased from PerkinElmer Life and Analytical Sciences (Waltham, MA).

Synthesis of POx block copolymers

Triblock copolymers, POx(A) (P[$MeOx_{34}$-*b*-$BuOx_{20}$-*b*-$MeOx_{35}$] (M_n = 8.6 kg/mol)), POx(B) (P[$MeOx_{38}$-*b*-$PpaOx_{27}$-*b*-$MeOx_{38}$] (M_n = 10.6 kg/mol)), POx(C) (P[$MeOx_{33}$-*b*-$BuOx_{21}$-*b*-$PpaOx_{29}$] (M_n = 9.9 kg/mol)), and POx(D) (P[$EtOx_{34}$-*b*-$BuOx_{21}$-*b*-$PpaOX_{31}$] (M_n = 10.7 kg/mol)) were synthesized by step-by-step (A-B-C) living cationic ring-opening polymerization (Scheme S1). Under dry and inert conditions, 1 equiv of MeOTf and pre-calculated equiv of corresponding block A monomer were dissolved in dry acetonitrile. The mixture was reacted in the microwave for 15min at 150 W and 130 °C. After cooling to room temperature, the monomer for block B was added and reacted again for another 15 min. The procedure was repeated with the monomer for block C and the polymerization was terminated by addition of 3 equiv of piperidine and incubating for 1hr at 50W and 40 °C. To remove the methyl ester group from P(MestOx), each polymer was dissolved in MeOH and mixed with 0.1N NaOH (1 eq to methyl ester group) at 90 °C for 3hr. The final solution was dialyzed (MWCO, 3500) against distilled water for 2 day and freeze-dried.

^{1}H NMR spectrum was obtained using INOVA 400 and analyzed using MestReNova (11.0) software. The spectra were calibrated using the MeOD solvent signals (4.78 ppm). The number-average molecular weight was determined by ^{1}H NMR, by calculating the ratio of the initiator and each repeating unit, using samples taken upon polymerization of each block and final block copolymer.

Preparation of drug loaded POx micelles

bioRxiv preprint doi: https://doi.org/10.1101/2021.06.09.447757; this version posted June 9, 2021. The copyright holder for this preprint (which was not certified by peer review) is the author/funder. All rights reserved. No reuse allowed without permission.

Drug-loaded polymeric micelles were prepared by thin-film hydration method as previously described. Each polymer and drug stock solutions in methanol were mixed together at the pre-determined ratios, followed by complete evaporation of methanol under a stream of nitrogen gas. The well-dried thin films were subsequently rehydrated with normal saline and then incubated at room temperature to self-assembly into drug-loaded polymeric micelles. The resulting micelle solutions were centrifuged at 10,000 g for 3 min (Sorvall Legend Micro 21R Centrifuge, Thermo Scientific) to remove non-loaded drug. The concentration of drugs in micelles were analyzed by reversed-phase high-pressure liquid chromatography (Agilent Technologies 1200 series) with a Nucleosil C18, 5 μm column (L × I.D. 250 mm × 4.6 mm). Samples were diluted 20 times in mobile phase (mixture of acetonitrile/water, with 0.01% trifluoroacetic acid) and 10 μL of the diluted sample was injected into the HPLC while the flow rate was 1.0 mL/min and column temperature was 40℃. The retention time of drugs, detection wavelength and detailed mobile phase were presented in **table S7**. The drug loading efficiency (LE) and loading capacity (LC) were calculated using following equations.

LE (%) = (weight of drugs in micelles) / (weight of drug initially added) ×100 % (1)

LC (%) = (weight of drugs in micelles) / (weight of micelles) ×100 % (2)

Characterization of drug loaded POx micelles

The particle size, polydispersity index (PDI) and zeta potential of drug loaded POx micelles were measured by photon correlation spectroscopy using a Zetasizer Nano-ZS (Malvern Instruments, Worcestershire, UK). Before measurement, each micelle was diluted to yield 1 mg/mL final polymer concentration and the average values were calculated from three independent sample measurements. To observe the morphologies of POx micelles, one drop of micelle solution

bioRxiv preprint doi: https://doi.org/10.1101/2021.06.09.447757; this version posted June 9, 2021. The copyright holder for this preprint (which was not certified by peer review) is the author/funder. All rights reserved. No reuse allowed without permission.

(diluted 100 times using distilled water) was placed on a copper grid/carbon film and stained with negative staining (1% uranyl acetate) prior to the TEM imaging.

The release profile of drug was determined as described earlier. Briefly, the POx-Palbo or Palbo-HCl were dispersed in saline (0.1 mg/ml of palbociclib), transferred into floatable Slide-A-Lyzer Mini dialysis device with 3.5 kDa (Thermo Fisher Scientific), and dialyzed against 20 mL PBS containing 10% FBS in compliance with the perfect sink conditions requirements. Four devices were used for each time points. At predetermined time points, the samples were collected and the remaining amount of palbociclib were analyzed by HPLC.

Animals

SmoM2$^{loxP/loxP}$ mice were purchased from the Jackson Laboratories (Bar Harbor, ME, USA). hGFAP-cre mice were generously provided by Dr. Eva Anton (University of North Carolina, Chapel Hill, NC, USA). Gli-luc mice, which express luciferase under the GLI promoter, were generously shared by Dr. Oren Becher and Dr. Eric Holland. Mouse genotyping was performed using Cre or SmoM2 primers. All mice were of the species Mus musculus and maintained on a C57BL/6 background over at least 5 generations. Mice were handled under the guidelines of a protocol approved by the University of North Carolina Institutional Animal Care and Use Committee (protocol 19-098).

Toxicology studies

MTD of POx-Palbo or Palbo-HCl were evaluated in healthy wildtype C57BL/6 mice. Pox-Palbo or Palbo-HCl was administered via intraperitoneal to group of 3 replicate mice on days P10-P14 and then every other day until P28. Mice at P12-21 are expected to continue to grow and gain weight. Age-matched littermate controls to determine the expected weight at each time point.

bioRxiv preprint doi: https://doi.org/10.1101/2021.06.09.447757; this version posted June 9, 2021. The copyright holder for this preprint (which was not certified by peer review) is the author/funder. All rights reserved. No reuse allowed without permission.

Signs of toxicity and associated behavior such as hunched posture, rough coat, and body weight changes were monitored daily. MTD was defined as the highest dose resulting in less than 15 % body weight changes compared to the control group. Healthy C57BL/6 mice received saline, Palbo-HCl 25 mg/kg, or POx-Palbo 25 mg/kg for 15 days (P10~P14: daily, P15~P24: every other day). The following day mice were sacrificed, and blood were collected and a comprehensive complete blood counts and blood chemistry panel were performed. Major organs including Heart, thymus, lung, liver, spleen and kidney were harvest, fixed in formalin, and subjected to pathological analysis by H&E staining.

Pharmacokinetic analysis

Groups of 3-4 replicate *G-Smo* mice were administered via intraperitoneal on P10 with a single dose of POx-Palbo or palbociclib-HCl at 25 mg/kg. All samples contained [3H] palbociclib (100 µci/kg). At various time points at 0.083, 2, 4, 8 and 24 hour post injections, three to four *G-Smo* mice from each groups were euthanized, and blood and organs (forebrain, tumor, liver, spleen, and kidney) were collected. Each organs were weighted and homogenized in 1 ml of Soluene-350. 50 µl of serum from each sample was collected and 1 ml of a mixture of soluene-350 and isopropyl alcohol at 1:1 ratio was added. A volume of 15 mL Ultima Gold LLC scintillation cocktail (PerkinElmer, USA) was added to each vial, vortexed, and counted in a liquid scintillation counter, Tricarb 4000 for [3H] palbociclib. Non-compartmental analysis (NCA) was performed using the Phoenix Winonlin software. Parameters derived from the NCA were used as initial estimates in the model building.

Efficacy studies

G-Smo mice were randomized into the indicated treatment groups with 4-12 replicate mice per group and administered via oral or intraperitoneal on P10 with each regimen. The indicated

bioRxiv preprint doi: https://doi.org/10.1101/2021.06.09.447757; this version posted June 9, 2021. The copyright holder for this preprint (which was not certified by peer review) is the author/funder. All rights reserved. No reuse allowed without permission.

formulations were administered until P35, unless mice first developed symptoms of tumor progression such as hunched posture, ataxia, tremor and seizures.

Pharmacodynamic analysis

P10-12 tumor mice were administered drugs (POx-Palbo, Palbo-HCl, POx-Sap, POx-(Palbo+Sap)) via intraperitoneal injections. EdU (40 mg/kg) was administered to mice thirty minutes before harvest. Tumor tissue was harvested and subjected to cellular dissociation via Worthington Papain Dissociation System kit. Dissociated Tumor cells were fixed for 15 minutes on ice. Washed with FACS wash buffer. Fixed cells were stained with fluorophore markers for DNA (FX Cycle stain, ThermoFisher Scientific, CAT #, F10347), EdU (Click-it Edu Kit, Thermofisher Scientific, CAT# C10337), and phoshpho-RB content (phospho-RB (Ser807/811), Cell Signaling Technology, CAT# 8974S). Stained cells were prepared in appropriate strained for flow analysis.

Flow Cytometry

Stained cells were resuspended ins Sheath Fluid and ran on a LSR II flow cytometer provided by the UNC Flow Cytometry Core. Proper compensation controls were used.

Immunofluorescence imaging

Brains including tumors from *G-Smo* pups were harvested, fixed in 4% paraformaldehyde for 48 hours, and embedded in paraffin at the UNC Center for Gastrointestinal Biology and Disease Histology core. Sections were deparaffinized, and antigen retrieval was performed using a low-pH citric acid-based buffer. Staining was performed and stained slides were digitally scanned using the Leica Biosystems Aperio ImageScope software (12.3.3) with assistance from the UNC Translational Pathology Laboratory. The primary antibodies used were anti-pRB (Cell Signaling

bioRxiv preprint doi: https://doi.org/10.1101/2021.06.09.447757; this version posted June 9, 2021. The copyright holder for this preprint (which was not certified by peer review) is the author/funder. All rights reserved. No reuse allowed without permission.

Technology, CAT # 8516), anti-p4EBP1 (Cell Signaling Technology, CAT #2855), anti-GLT1 (Thermofisher Scientific, CAT #701988).

Drop-Seq library preparation, sequencing, and analysis

We used Drop-seq (*23*) methods for scRNA sequence study as in our prior studies (*17, 22*). Briefly, Drop-seq libraries were prepared according to the Drop-seq protocol V 3.1 (Ref 32), with full details available online (http://mccarrolllab.com/dropseq/). Cell and bead concentrations were both set to between 95 and 110/μL. Tumor cells were co-encapsulated using a Dolomite-brand glass device. All cells were processed within 1 h of tissue dissociation. Flow rates on the glass device were set to 2400 and 12,000 μL/h for cells/beads and oil, respectively, with a 1–2.5% bead occupancy rate. From the obtained library, the raw sequence data were processed in a Linux environment using Drop-seq Tools V1.13 (https://github.com/broadinstitute/Drop-seq/releases) to generate a digital expression (DGE) matrix. DGE matrices were used to generate Seurat objects in R (https://satijalab.org/seurat/). Input data are raw sequences in Fastq format, demultiplexed by sample identity. We first convert Fastq to BAM/SAM format and merge samples that were sequenced across multiple lanes. Data analysis was performed in an R environment using the Seurat toolkit. After filtering the data by QC criteria, genes were selected for differential expression across the sample using Seurat's highly variable gene selection tool, "FindVariableGenes". Mean expression and variance was calculated across the sample, and mean expression plotted against dispersion (variance/mean). PCA was used to reduce the dimensionality of the gene expression matrix.

bioRxiv preprint doi: https://doi.org/10.1101/2021.06.09.447757; this version posted June 9, 2021. The copyright holder for this preprint (which was not certified by peer review) is the author/funder. All rights reserved. No reuse allowed without permission.

SUPPLEMENTARY MATERIALS

Fig. S1. Scheme of the synthesis of POx block copolymer to be used to prepared POx-micelles.

Fig. S2. Dynamic flow cytometry cell-cycle gating strategy in medulloblastoma-bearing mice.

Fig. S3. (A) Characterization of drug loaded POx micelles. (B-D) Toxicity studies in C57BL/6 mice. The weights of mice treated with (B) Gemcitabine, (C) POx-Etoposide, and (C) POx-Sapanisertib over time. The gray range indicates the mean weights of ± SEM of littermate controls.

Fig. S4. Characterization of (A) POx-(Palbociclib+Vismodegib), (B) POx-(Palbociclib+Etoposide), and (C) POx-(Palbociclib+Sapanisertib) including particle size distribution, zeta potential, and morphology. (D) Particle size, PDI, loading capacity and loading efficiency of two-drug loaded POx micelles.

Table S1. PK parameters of palbociclib in liver, kidney and spleen.

Table S2. Palbociclib regimens used in *in vivo* testing.

Table S3. Palbociclib+vismodegib regimens used in *in vivo* testing.

Table S4. Palbociclib+gemcitabine regimens used in *in vivo* testing.

Table S5. Palbociclib+etoposide regimens used in *in vivo* testing.

Table S6. Palbociclib+Sapanisertib regimens used in *in vivo* testing.

Table S7. HPLC conditions for analyzing the drug concentration in POx micelle.

Data file S1. Gene expression changes and GO analysis.

Acknowledgments

We thank the UNC CGBID Histology Core supported by P30 DK 034987, the UNC Tissue Pathology Laboratory Core supported by NCI CA016086 and UNC UCRF, and the Chapel Hill Analytical and Nanofabrication Laboratory, supported by the National Science Foundation Grant ECCS-1542015, for help with electron microscopy.

Funding

This work was supported by the NCI Alliance for Nanotechnology in Cancer (U54CA198999, Carolina Center of Cancer Nanotechnology Excellence), by NINDS (R01NS088219, R01NS102627, R01NS106227) and by the St. Baldrick's Foundation.

Author contributions

bioRxiv preprint doi: https://doi.org/10.1101/2021.06.09.447757; this version posted June 9, 2021. The copyright holder for this preprint (which was not certified by peer review) is the author/funder. All rights reserved. No reuse allowed without permission.

Conceptualization: CL, TD, TRG, MSP, AVK; Methodology: CL, TD, VLG, DM, JDR, DH; Investigation: CL, TD, VLG, DM; Visualization: CL, TD; Funding acquisition: TRG, MSP; Project administration: TRG, MSP; Supervision: TRG, MSP, AVK; Writing – original draft: CL, TD; Writing – review & editing: TRG, MSP.

Competing interests

A.V.K. is a co-inventor on patents pertinent to the subject matter of the present contribution, and A.V.K. and M.S.P. have co-founders interest in DelAqua Pharmaceuticals Inc., having intent of commercial development of POx-based drug formulations. A.V.K. is a co-inventor of the U.S. Patent # 9,402,908 B2 and may have certain rights to this invention. The other authors declare that they have no competing interests.

Data and materials availability

All data are available in the main text or the supplementary materials.

References and Notes

1. D. R. Raleigh, P. K. Choksi, A. L. Krup, W. Mayer, N. Santos, J. F. Reiter, Hedgehog signaling drives medulloblastoma growth via CDK6. *J Clin Invest* **128**, 120-124 (2018).
2. M. L. Cook Sangar, L. A. Genovesi, M. W. Nakamoto, M. J. Davis, S. E. Knobluagh, P. Ji, A. Millar, B. J. Wainwright, J. M. Olson, Inhibition of CDK4/6 by Palbociclib Significantly Extends Survival in Medulloblastoma Patient-Derived Xenograft Mouse Models. *Clin Cancer Res* **23**, 5802-5813 (2017).
3. D. W. Parsons, M. Li, X. Zhang, S. Jones, R. J. Leary, J. C. Lin, S. M. Boca, H. Carter, J. Samayoa, C. Bettegowda, G. L. Gallia, G. I. Jallo, Z. A. Binder, Y. Nikolsky, J. Hartigan, D. R. Smith, D. S. Gerhard, D. W. Fults, S. VandenBerg, M. S. Berger, S. K. Marie, S. M. Shinjo, C. Clara, P. C. Phillips, J. E. Minturn, J. A. Biegel, A. R. Judkins, A. C. Resnick, P. B. Storm, T. Curran, Y. He, B. A. Rasheed, H. S. Friedman, S. T. Keir, R. McLendon, P. A. Northcott, M. D. Taylor, P. C. Burger, G. J. Riggins, R. Karchin, G. Parmigiani, D. D. Bigner, H. Yan, N. Papadopoulos, B. Vogelstein, K. W. Kinzler, V. E. Velculescu, The genetic landscape of the childhood cancer medulloblastoma. *Science* **331**, 435-439 (2011).
4. P. A. Northcott, D. J. Shih, J. Peacock, L. Garzia, A. S. Morrissy, T. Zichner, A. M. Stutz, A. Korshunov, J. Reimand, S. E. Schumacher, R. Beroukhim, D. W. Ellison, C. R. Marshall, A. C. Lionel, S. Mack, A. Dubuc, Y. Yao, V. Ramaswamy, B. Luu, A. Rolider, F. M. Cavalli, X. Wang, M. Remke, X. Wu, R. Y. Chiu, A. Chu, E. Chuah, R. D. Corbett, G. R. Hoad, S. D. Jackman, Y. Li, A. Lo, K. L. Mungall, K. M. Nip, J. Q. Qian, A. G. Raymond, N. T. Thiessen, R. J. Varhol, I. Birol, R. A. Moore, A. J. Mungall, R. Holt, D. Kawauchi, M. F. Roussel, M. Kool, D. T. Jones, H. Witt, L. A. Fernandez, A. M. Kenney, R. J. Wechsler-Reya, P. Dirks, T. Aviv, W. A. Grajkowska, M. Perek-Polnik, C. C. Haberler, O. Delattre, S. S. Reynaud, F. F. Doz, S. S. Pernet-Fattet, B. K. Cho, S. K. Kim, K. C. Wang, W. Scheurlen, C. G. Eberhart, M. Fevre-Montange, A. Jouvet, I. F. Pollack, X. Fan, K. M. Muraszko, G. Y. Gillespie, C. Di Rocco, L. Massimi, E. M. Michiels, N. K. Kloosterhof, P. J. French, J. M. Kros, J. M. Olson, R. G. Ellenbogen, K. Zitterbart, L. Kren, R. C. Thompson, M. K. Cooper, B. Lach, R. E. McLendon, D. D. Bigner, A. Fontebasso, S. Albrecht, N. Jabado, J. C. Lindsey, S. Bailey, N. Gupta, W. A. Weiss, L. Bognar, A. Klekner, T. E. Van Meter, T. Kumabe, T. Tominaga, S. K. Elbabaa, J. R. Leonard, J. B. Rubin, L. M. Liau, E. G. Van Meir, M. Fouladi, H. Nakamura, G. Cinalli, M. Garami, P. Hauser, A. G. Saad, A. Iolascon, S. Jung, C. G. Carlotti, R. Vibhakar, Y. S. Ra, S. Robinson, M. Zollo, C. C. Faria, J. A. Chan, M. L. Levy, P. H. Sorensen, M. Meyerson, S. L. Pomeroy, Y. J. Cho, G. D. Bader, U. Tabori, C. E. Hawkins, E. Bouffet, S. W. Scherer, J. T. Rutka, D. Malkin, S. C. Clifford, S. J. Jones, J. O. Korbel, S. M. Pfister, M. A. Marra, M. D. Taylor, Subgroup-specific structural variation across 1,000 medulloblastoma genomes. *Nature* **488**, 49-56 (2012).
5. M. Kool, A. Korshunov, M. Remke, D. T. Jones, M. Schlanstein, P. A. Northcott, Y. J. Cho, J. Koster, A. Schouten-van Meeteren, D. van Vuurden, S. C. Clifford, T. Pietsch, A. O. von Bueren, S. Rutkowski, M.

bioRxiv preprint doi: https://doi.org/10.1101/2021.06.09.447757; this version posted June 9, 2021. The copyright holder for this preprint (which was not certified by peer review) is the author/funder. All rights reserved. No reuse allowed without permission.

McCabe, V. P. Collins, M. L. Backlund, C. Haberler, F. Bourdeaut, O. Delattre, F. Doz, D. W. Ellison, R. J. Gilbertson, S. L. Pomeroy, M. D. Taylor, P. Lichter, S. M. Pfister, Molecular subgroups of medulloblastoma: an international meta-analysis of transcriptome, genetic aberrations, and clinical data of WNT, SHH, Group 3, and Group 4 medulloblastomas. *Acta Neuropathol* **123**, 473-484 (2012).

6. D. W. Fry, P. J. Harvey, P. R. Keller, W. L. Elliott, M. Meade, E. Trachet, M. Albassam, X. Zheng, W. R. Leopold, N. K. Pryer, P. L. Toogood, Specific inhibition of cyclin-dependent kinase 4/6 by PD 0332991 and associated antitumor activity in human tumor xenografts. *Mol Cancer Ther* **3**, 1427-1438 (2004).
7. N. C. Turner, J. Ro, F. Andre, S. Loi, S. Verma, H. Iwata, N. Harbeck, S. Loibl, C. Huang Bartlett, K. Zhang, C. Giorgetti, S. Randolph, M. Koehler, M. Cristofanilli, P. S. Group, Palbociclib in Hormone-Receptor-Positive Advanced Breast Cancer. *N Engl J Med* **373**, 209-219 (2015).
8. R. S. Finn, J. P. Crown, I. Lang, K. Boer, I. M. Bondarenko, S. O. Kulyk, J. Ettl, R. Patel, T. Pinter, M. Schmidt, Y. Shparyk, A. R. Thummala, N. L. Voytko, C. Fowst, X. Huang, S. T. Kim, S. Randolph, D. J. Slamon, The cyclin-dependent kinase 4/6 inhibitor palbociclib in combination with letrozole versus letrozole alone as first-line treatment of oestrogen receptor-positive, HER2-negative, advanced breast cancer (PALOMA-1/TRIO-18): a randomised phase 2 study. *Lancet Oncol* **16**, 25-35 (2015).
9. T. J. Raub, G. N. Wishart, P. Kulanthaivel, B. A. Staton, R. T. Ajamie, G. A. Sawada, L. M. Gelbert, H. E. Shannon, C. Sanchez-Martinez, A. De Dios, Brain Exposure of Two Selective Dual CDK4 and CDK6 Inhibitors and the Antitumor Activity of CDK4 and CDK6 Inhibition in Combination with Temozolomide in an Intracranial Glioblastoma Xenograft. *Drug Metab Dispos* **43**, 1360-1371 (2015).
10. M. Malumbres, R. Sotillo, D. Santamaria, J. Galan, A. Cerezo, S. Ortega, P. Dubus, M. Barbacid, Mammalian cells cycle without the D-type cyclin-dependent kinases Cdk4 and Cdk6. *Cell* **118**, 493-504 (2004).
11. M. Malumbres, CDK4/6 Inhibitors: What Is the Best Cocktail? *Clin Cancer Res* **25**, 6-8 (2019).
12. K. L. Barton, K. Misuraca, F. Cordero, E. Dobrikova, H. D. Min, M. Gromeier, D. G. Kirsch, O. J. Becher, PD-0332991, a CDK4/6 inhibitor, significantly prolongs survival in a genetically engineered mouse model of brainstem glioma. *PLoS One* **8**, e77639 (2013).
13. J. W. Taylor, M. Parikh, J. J. Phillips, C. D. James, A. M. Molinaro, N. A. Butowski, J. L. Clarke, N. A. Oberheim-Bush, S. M. Chang, M. S. Berger, M. Prados, Phase-2 trial of palbociclib in adult patients with recurrent RB1-positive glioblastoma. *J Neurooncol* **140**, 477-483 (2018).
14. D. Hwang, J. D. Ramsey, A. V. Kabanov, Polymeric micelles for the delivery of poorly soluble drugs: From nanoformulation to clinical approval. *Adv Drug Deliv Rev*, (2020).
15. P. Y. Lang, G. J. Nanjangud, M. Sokolsky-Papkov, C. Shaw, D. Hwang, J. S. Parker, A. V. Kabanov, T. R. Gershon, ATR maintains chromosomal integrity during postnatal cerebellar neurogenesis and is required for medulloblastoma formation. *Development* **143**, 4038-4052 (2016).
16. D. Hwang, T. Dismuke, A. Tikunov, E. P. Rosen, J. R. Kagel, J. D. Ramsey, C. Lim, W. Zamboni, A. V. Kabanov, T. R. Gershon, D. M. Sokolsky-Papkov Ph, Poly(2-oxazoline) nanoparticle delivery enhances the therapeutic potential of vismodegib for medulloblastoma by improving CNS pharmacokinetics and reducing systemic toxicity. *Nanomedicine* **32**, 102345 (2020).
17. D. Malawsky, S. J. Weir, J. Ocasio, B. Babcock, T. Dismuke, K. Wilhelmsen, T. R. Gershon, Cryptic developmental events determine medulloblastoma radiosensitivity and cellular heterogeneity without altering transcriptomic profile. *PREPRINT (Version 1) available at Research Square*, (2020).
18. T. R. Gershon, A. J. Crowther, A. Tikunov, I. Garcia, R. Annis, H. Yuan, C. R. Miller, J. Macdonald, J. Olson, M. Deshmukh, Hexokinase-2-mediated aerobic glycolysis is integral to cerebellar neurogenesis and pathogenesis of medulloblastoma. *Cancer Metab* **1**, (2013).
19. U. Schüller, V. M. Heine, J. Mao, A. T. Kho, A. K. Dillon, Y.-G. Han, E. Huillard, T. Sun, A. H. Ligon, Y. Qian, Q. Ma, A. Alvarez-Buylla, A. P. McMahon, D. H. Rowitch, K. L. Ligon, Acquisition of Granule Neuron Precursor Identity Is a Critical Determinant of Progenitor Cell Competence to Form Shh-Induced Medulloblastoma. *Cancer Cell* **14**, 123-134 (2008).
20. M. Longmire, P. L. Choyke, H. Kobayashi, Clearance properties of nano-sized particles and molecules as imaging agents: considerations and caveats. *Nanomedicine (Lond)* **3**, 703-717 (2008).
21. O. J. Becher, D. Hambardzumyan, E. I. Fomchenko, H. Momota, L. Mainwaring, A. M. Bleau, A. M. Katz, M. Edgar, A. M. Kenney, C. Cordon-Cardo, R. G. Blasberg, E. C. Holland, Gli activity correlates with tumor grade in platelet-derived growth factor-induced gliomas. *Cancer Res* **68**, 2241-2249 (2008).
22. J. Ocasio, B. Babcock, D. Malawsky, S. J. Weir, L. Loo, J. M. Simon, M. J. Zylka, D. Hwang, T. Dismuke, M. Sokolsky, E. P. Rosen, R. Vibhakar, J. Zhang, O. Saulnier, M. Vladoiu, I. El-Hamamy, L. D. Stein, M. D. Taylor, K. S. Smith, P. A. Northcott, A. Colaneri, K. Wilhelmsen, T. R. Gershon, scRNA-seq in

bioRxiv preprint doi: https://doi.org/10.1101/2021.06.09.447757; this version posted June 9, 2021. The copyright holder for this preprint (which was not certified by peer review) is the author/funder. All rights reserved. No reuse allowed without permission.

medulloblastoma shows cellular heterogeneity and lineage expansion support resistance to SHH inhibitor therapy. *Nat Commun* **10**, 5829 (2019).

23. E. Z. Macosko, A. Basu, R. Satija, J. Nemesh, K. Shekhar, M. Goldman, I. Tirosh, A. R. Bialas, N. Kamitaki, E. M. Martersteck, J. J. Trombetta, D. A. Weitz, J. R. Sanes, A. K. Shalek, A. Regev, S. A. McCarroll, Highly Parallel Genome-wide Expression Profiling of Individual Cells Using Nanoliter Droplets. *Cell* **161**, 1202-1214 (2015).
24. L. Z. Loo, M, Drop seq brain. *Nat Commun*, (2019).
25. M. C. Vladoiu, I. El-Hamamy, L. K. Donovan, H. Farooq, B. L. Holgado, V. Ramaswamy, S. C. Mack, J. J. Y. Lee, S. Kumar, D. Przelicki, A. MichaelRaj, K. Juraschka, P. Skowron, B. Luu, H. Suzuki, S. A. Morrissy, F. M. G. Cavalli, L. Garzia, C. Daniels, X. Wu, M. A. Qazi, S. K. Singh, J. A. Chan, M. A. Marra, D. Malkin, P. Dirks, T. Pugh, F. Notta, C. L. Kleinman, A. Joyner, N. Jabado, L. Stein, M. D. Taylor, Childhood cerebellar tumors mirror conserved fetal transcriptional programs. *bioRxiv*, 350280 (2018).
26. M. D. Luecken, F. J. Theis, Current best practices in single-cell RNA-seq analysis: a tutorial. *Mol Syst Biol* **15**, e8746 (2019).
27. V. Iadevaia, R. Liu, C. G. Proud, mTORC1 signaling controls multiple steps in ribosome biogenesis. *Semin Cell Dev Biol* **36**, 113-120 (2014).
28. S. Barua, J.-W. Yoo, P. Kolhar, A. Wakankar, Y. R. Gokarn, S. Mitragotri, Particle shape enhances specificity of antibody-displaying nanoparticles. *Proceedings of the National Academy of Sciences* **110**, 3270-3275 (2013).
29. C. C. Wu, S. Hou, B. A. Orr, B. R. Kuo, Y. H. Youn, T. Ong, F. Roth, C. G. Eberhart, G. W. Robinson, D. J. Solecki, M. M. Taketo, R. J. Gilbertson, M. F. Roussel, Y. G. Han, mTORC1-Mediated Inhibition of 4EBP1 Is Essential for Hedgehog Signaling-Driven Translation and Medulloblastoma. *Dev Cell* **43**, 673-688 e675 (2017).
30. M. Y. Wan X, Bludau H, Keith A, Sheiko S, Jordan R, Wang A, Sokolsky-Papkov M, Kabanov AV, Drug Combination Synergy in Worm-Like Polymeric Micelles Improves Treatment Outcome for Small Cell and Non-Small Cell Lung Cancer. *ACS Nano* **in press**, (2018).
31. Y. Han, Z. He, A. Schulz, T. K. Bronich, R. Jordan, R. Luxenhofer, A. V. Kabanov, Synergistic combinations of multiple chemotherapeutic agents in high capacity poly(2-oxazoline) micelles. *Mol Pharm* **9**, 2302-2313 (2012).
32. V. Daggubati, J. Hochstelter, A. Bommireddy, A. Choudhury, A. L. Krup, P. Kaur, P. Tong, A. Li, L. Xu, J. F. Reiter, D. R. Raleigh, Smoothened-activating lipids drive resistance to CDK4/6 inhibition in Hedgehog-associated medulloblastoma cells and preclinical models. *J Clin Invest* **131**, (2021).
33. X. Song, X. Liu, H. Wang, J. Wang, Y. Qiao, A. Cigliano, K. Utpatel, S. Ribback, M. G. Pilo, M. Serra, J. D. Gordan, L. Che, S. Zhang, A. Cossu, A. Porcu, R. M. Pascale, F. Dombrowski, H. Hu, D. F. Calvisi, M. Evert, X. Chen, Combined CDK4/6 and Pan-mTOR Inhibition Is Synergistic Against Intrahepatic Cholangiocarcinoma. *Clin Cancer Res* **25**, 403-413 (2019).